11:51:17 OCA PAD INITIATION - PROJECT HEADER INFORMATION 11/01/88

Active

Project #: E-25-622
Center # : R6531-0A1
Cost share #:
Center shr #:
Rev #: 0
OCA file #:
Work type : RES
Document : GRANT
Contract entity: GTRC

Contract#: ATM-8896213
Mod #: MEMO M HAYES
Prime #:

Subprojects ? : N
Main project #: B-10-648

Project unit: ME Unit code: 02.010.126
Project director(s):
HAYES M A ME (404)894-3720

Sponsor/division names: NATL SCIENCE FOUNDATION / GENERAL
Sponsor/division codes: 107 / 000

Award period: 880301 to 881231 (performance) 890331 (reports)

Sponsor amount	New this change	Total to date
Contract value	45,000.00	45,000.00
Funded	45,000.00	45,000.00
Cost sharing amount		0.00

Does subcontracting plan apply ?: N

Title: INVESTIGATION OF CURRENT DIVISION IN A STRONGLY MAGNETIZED LABORATORY PLASMA

PROJECT ADMINISTRATION DATA

OCA contact: Steven K. Watt 894-4820

Sponsor technical contact

DENNIS PEACOCK
(202)357-7618
NATIONAL SCIENCE FOUNDATION
AEO/ATM
WASHINGTON, D.C. 20550

Sponsor issuing office

JODI CONDES
(202)357-9602
NATIONAL SCIENCE FOUNDATION
DGC/AEO
WASHINGTON, D.C. 20550

Security class (U,C,S,TS) : U
Defense priority rating : N/A
Equipment title vests with: Sponsor GIT X
EQUIPMENT TRANSFERRED FROM DARTMOUTH COLLEGE

ONR resident rep. is ACO (Y/N): N
NSF supplemental sheet

Administrative comments -
SUBPROJECT SET-UP UNDER B-10-648 TO TRANSFER PROJECT FROM OIP TO MECH ENG.
ALL FUNDS AND DELIVERABLES ARE ACCOUNTABLE UNDER SUBPROJECT.

SR 20? 29

GEORGIA INSTITUTE OF TECHNOLOGY
OFFICE OF CONTRACT ADMINISTRATION

NOTICE OF PROJECT CLOSEOUT

Date 8/23/89

oject No. E-25-622 Center No. R6531-0A1

oject Director M. A. Hayes School/Lab ME

onsor National Science Foundation

itract/Grant No. ATM-8896213 GTRC XX GIT ___

ime Contract No. N/A

:le Investigation of Current Division in a Strongly Magnetized Laboratory Plasma

ective Completion Date 12/31/88 (Performance) 3/31/89 (Reports)

oseout Actions Required:

_ None
_ Final Invoice or Copy of Last Invoice
_ Final Report of Inventions and/or Subcontracts
_ Government Property Inventory & Related Certificate
_ Classified Material Certificate
_ Release and Assignment
_ Other ______

ludes Subproject No(s). ______

oproject Under Main Project No. B-10-648/Hayes/ME

tinues Project No. ______ Continued by Project No. ______

tribution:

- Project Director
- Administrative Network
- Accounting
- Procurement/GTRI Supply Services
- Research Property Management
- Research Security Services
- X Reports Coordinator (OCA)
- X GTRC
- X Project File
- X Contract Support Division (OCA)
- ___ Other ______

E-25-622

APPENDIX VII

NATIONAL SCIENCE FOUNDATION
Washington, D.C. 20550

FINAL PROJECT REPORT
NSF FORM 98A

PART I—PROJECT IDENTIFICATION INFORMATION

1. Institution and Address	2. NSF Program	3. NSF Award Number
Georgia Tech Atlanta, Ga. 30332	Atmospheric	ATM-8896213
	4. Award Period From 88:03/01 To 88:12/31	5. Cumulative Award Amount $45,000.00

6. Project Title
Investigation of Current Division in a Strongly Magnetized Laboratory Plasma

PART II—SUMMARY OF COMPLETED PROJECT *(FOR PUBLIC USE)*

See attached page

PART III—TECHNICAL INFORMATION *(FOR PROGRAM MANAGEMENT USES)*

1. ITEM *(Check appropriate blocks)*	NONE	ATTACHED	PREVIOUSLY FURNISHED	TO BE FURNISHED SEPARATELY TO PROGRAM: Check (✓)	Approx. Date
a. Abstracts of Theses					
b. Publication Citations					
c. Data on Scientific Collaborators					
d. Information on Inventions					
e. Technical Description of Project and Results					
f. Other *(specify)*					

2. Principal Investigator/Project Director Name *(Typed)*	3. Principal Investigator/Project Director Signature	4. Date
Michael Hayes		7/10/89

NSF Form 98A (1-87) Supersedes All Previous Editions

Form Approved OMB No. 3145-0058

Summary of the Completed Project:

Investigation of Current Driven Double Layers in a Strongly Magnetized Laboratory Plasma

Michael A. Hayes
Senior Research Scientist
Nuclear Engineering Program
Georgia Institute of Technology
Atlanta, GA 30332

Double layers are interesting examples of non-linear plasma processes, and are believed to play an important role in determining the physical behavior of the earth's auroral acceleration region. The research in which our group has conducted has produced a number of interesting and significant results do date. Our work has demonstrated the rapid growth of transverse double layers under a variety of current and plasma drift conditions, and in both helium and argon plasmas. We have also obtained indications of soliton-like transverse triple layers, and we have obtained rough frequency spectrum information on a number of non-linear potential and density structures. In order to perform this work to the degree of accuracy desired, we made a number of developments in plasma technology, including improved plasma sources, and improved diagnostic techniques; we even made some improvements in vacuum technology. The plasmas in which our experiments have been performed have been carefully characterized. Both electron temperature and plasma drift speed determinations have been made by launching ion acoustic waves in both axial directions, and taking both sums and differences of the wavelengths. Absolute determinations of radial density profile have been achieved by benchmarking ion saturation probes to a microwave resonance shift density measuring cavity. It was this radial density profile information which first led us to suspect the importance of drift waves in transverse potential structure formation. We have begun to address the question of the roles played in transverse double layers by drift waves, and also by electrostatic ion cyclotron waves, and we have determined that an interaction between these wave types is part of the transverse double layer formation process. While noting the rapid rate of growth of transverse double layers and other potential structures, we have also established an upper bound of about (0.1)eV, ie. about $(.03)T_e$ (where T_e is the electron temperature), for the potential jump of frequently occurring axial double layers. That is to say, we have determined that axial double layers are either rarer, or smaller, than had been expected, while transverse double layers were found to be more robust than expected.

Synopsis of Results to Date

One important feature which became evident during the course of our research was that the potential and density structures which have the fastest growth rates are almost completely transverse to the magnetic field, ie. $k_\perp >> k_\parallel$. I spent a great deal of time and effort trying to discover some parameter regime in which I could accurately measure the $k_\parallel$ components of a potential structure, but this is quite difficult, as all of the structures so far observed have a parallel phase velocity in excess of a tenth of the electron thermal velocity, $(0.1)v_e$, which is the limit on parallel phase velocity which currently applies to my measurement ability. This is not a hard and fast limit, but rather results from the finite length of the tank in combination with the limits on my ability to resolve the phase of a structure as it moves past the probes. Parallel phase velocities much below $(0.1)v_e$ could be well resolved if any of the structures observed had parallel velocities in this range, but none do. In particular it is quite clear that the parallel phase velocity of the structures so far observed greatly exceed the ion acoustic speed. We can try establish an upper bound to the size of axially propagating structures which might be hiding in the data plates, unobserved by us. My best guess at the upper bound on axially propagating double layers which might be frequently occuring, but undetected within the data, is roughly 0.1 eV, which corresponds to less than one thirtieth of the electron temperature.

This was quite different from what I had anticipated and, if anything, more interesting. In order to obtain some input from theoreticians working on this problem, I sent copies of some of my experimental data, with explanations and guides to interpretation, to two well respected theoreticians working in this field, Dr. Tom Chang of the Center for Space Research, at MIT, and Dr. Mary Hudson of the Department of Physics, Dartmouth.

After observing the data, Dr. Chang suggested that it appears that non-linear Electrostatic Ion Cyclotron (EIC) waves are involved. According to this theoretical interpretation, my experimental observations could be the result of non-linear EIC wave propatation very nearly perpendicular to the magnetic field. Because the wave is electrostatic, the electric field would then also be in the transverse direction, which would explain the polarization of the resulting double layers. After hearing Dr. Chang's interpretation of these results, I compared my rough observations of the frequency components of the observed transverse double layers with what might be expected from EIC waves. The resulting comparison was interesting and significant; it is presented below.

As noted in the section on experimental results, the frequency components of these waves range down to a tenth of the ion cyclotron frequency. This is inconsistent with the approximate form of the EIC dispersion relation which is frequently presented, for example in Nicholson, ie.:

$$\omega^2 = k^2 c_s^2 + \Omega_i^2$$

where ω is the angular frequency of the wave, k is the magnitude of the wave vector, c_s is the ion acoustic speed, and Ω_i is the angular ion gyro frequency. But this approximate form ignores a term which will be important as the propagation angle approaches perpendicularity to the magnetic field. Retaining this term, gives:

$$\omega^2 = (k^2 c_s^2 + \Omega_i^2) \Big/ [1 + (m_e/M_i)(k_\perp/k_\parallel)^2]$$

where m_e and M_i are the electron and ion masses, respectively, and $k_\perp$ and $k_\parallel$ are respectively the perpendicular and parallel components of the wave vector (and hence $k_\perp^2 + k_\parallel^2 = k^2$). This indicates that EIC waves below the ion cyclotron frequency can propagate, but only at angles very nearly perpendicular to the magnetic field, which is just what we observe.

Manipulation of the this more exact dispersion relation gives:

$$\omega^2 [1 + (m_e/M_i)(k_\perp/k_\parallel)^2] = (k_\perp^2 + k_\parallel^2) c_s^2 + \Omega_i^2$$

where we have used the identity $k_\perp^2 + k_\parallel^2 = k^2$. Subtracting ω^2 from both sides gives:

$$\omega^2 (m_e/M_i)(k_\perp/k_\parallel)^2] = (k_\perp^2 + k_\parallel^2)c_s^2 + (\Omega_i^2 - \omega^2)$$

Dividing both sides by $(m_e/M_i)k_\perp^2$ gives the expression:

$$(\omega/k_\parallel)^2 = (M_i/m_e)\,[\{1 + (k_\parallel/k_\perp)^2\}\,c_s^2 + (\Omega_i^2 - \omega^2)/\,k_\perp^2]$$

Defining the parallel and perpendicular components of the phase velocities: $v_\parallel = (\omega/k_\parallel)$, and $v_\perp = (\omega/k_\perp)$ allows us to rewrite the above expression as:

$$v_\parallel^2 = (M_i/m_e)\,[\{1 + (v_\perp/v_\parallel)^2\}\,c_s^2 + (\Omega_i^2 - \omega^2)/\,k_\perp^2]$$

Since our experimental observations have always indicated $v_\perp << v_\parallel$, we may approximate:

$$v_\parallel^2 \approx (M_i/m_e)c_s^2 + (M_i/m_e)(\Omega_i^2 - \omega^2)/\,k_\perp^2$$

or, since $(M_i/m_e)c_s^2 = v_e^2$, where v_e is the electron thermal velocity:

$$v_\parallel^2 \approx v_e^2 + (M_i/m_e)(\Omega_i^2 - \omega^2)/\,k_\perp^2$$

or:

$$v_\parallel^2 \approx v_e^2\,[1 + (M_i/m_e)(\Omega_i^2 - \omega^2)/(v_e^2 k_\perp^2)]$$

Typical experiments conducted in Argon plasmas in a 540G magnetic field gave a temperature of 3.5 eV, and a fairly wide range of $k_\perp$ values, with $k_\perp \approx 25\text{m}^{-1}$ frequently occurring. Combining this $k_\perp$ value and temperature with the requisite fundamental constants and grinding gives:

$$v_\parallel \approx (1.12)\,v_e$$

which not only is consistent with the fact that the parallel phase velocity is too large for us to measure directly, but also is a phase velocity at which inverse Landau damping on the tail electrons from our hammer source may be a possibility. Inverse Landau damping may play a role in determining the fastest growing modes, and the fact that the nearly perpendicular (to the magnetic field) EIC modes have a parallel phase velocity which automatically falls in a range of values well situated to enjoy inverse Landau damping <u>may</u> explain why they such waves appear to dominate in our experiment over waves with parallel phase velocity in the range of the ion acoustic speed. Another possible explanation of this observation, presented below, has the energy for growth of EIC waves coming from drift waves, and has the EIC waves subsequently <u>losing</u> energy via Landau damping on the electrons. Not only a better determination of the parallel electron distribution function, but also a better determination of the radial and azimuthal components of the wave electric field and density gradient are needed.

Other wave components in argon give values in the range

$$v_e < v_\parallel < (1.25)\,v_e$$

The helium plasmas produced were typically a little bit warmer than the argon plasmas, averaging around 4.2 eV (probably due to the higher ionization potential of Helium than of Argon). The helium experiments produced frequencies typically a tenth of the helium gyrofrequency, but with less variation about the typical value than was observed with Argon. Similarly, the variation in observed $k_\perp$ values was also smaller, which results in a more tightly clustered set of inferred $v_{||}$ values. For helium, we typically found:

$$v_{||} \approx (1.1)\, v_e$$

All in all, the radially outward propagation of EIC waves seems to be consistent with all observations to date, and also to make sense of the observed spectrum of both ω and $k_\perp$ values.

The theory of drift waves, however, also seems to have something to contribute to our understanding of the observed spectra. For a perfectly symmetric plasma column, drift waves should be purely azimuthal, but even the slightly imperfect symmetry shown in our density profiles (see density profile figures), could give rise to the radial electric fields which we appear to be observing. Even more important, with our present set of probe tips (which were optimized, according to our thoughts at the time, to make fine distinctions in parallel structure), we are unable to determine with certainty whether we are observing radial propagation which would be characteristic of EIC waves, or very strongly sheared propagation in the azimuthal direction (that is, azimuthal propagation in which the rotation frequency of an annulus was strongly dependent on its radius), which would be characteristic of drift waves, or perhaps a combination of the two. The present probe tips were designed to be able to distinguish transverse propagation from axial propagation, but they were not designed to make the further distinction between radial and azimuthal propagation. The set of experiments herein proposed will dispose of this uncertainty, but at present this uncertainty is very real, particularly in light of the fact that the numerical values of the fastest growing drift modes for our tank geometry correspond so well to the modes we see. For example, from Schmidt we get:

$$v_d = v_e R_e(-d/dx \ln n)$$

for a plasma with a gradient in the x direction, where v_d is the diamagnetic drift velicity, and R_e is the electron Larmour radius. Corrections due to the fact that our plasma geometry is cylindrical are unimportant here, as we are merely trying to estimate magnitudes, so we can use $(-d/dx \ln n) \approx 0.5\text{cm}^{-1}$, which may be obtained from the plot of $(d/dr \ln n)$ which is given (see figure). As noted above, the temperature of the typical argon plasma is about 3.5 eV while the typical helium plasma runs about 4.2 eV; in the spirit of approximation, we may use the average of these quantities to get an average electron thermal velocity of $v_e \approx 8.2 \times 10^5$ m/s, and an average electron Larmour radius at 540G of $R_e \approx 8.5 \times 10^{-3}$ cm. All of this gives:

$$v_d \approx 3.5 \times 10^3 \text{ m/s}$$

Also from Schmidt, we find that the dispersion relation in the limit of small $k_{||}$ is approximately given by:

$$\omega \approx k_\perp v_d / \sigma$$

where $\sigma = 1 + c_s^2 k_\perp^2 / \Omega_i^2$. Schmidt goes on to point out that the fastest growing drift waves are characterized by $\sigma \approx 3$, which gives the phase velocity of the fastest growing modes in the neighborhood:

$$\omega / k_\perp \approx 1.2 \times 10^3 \text{ m/s}$$

which is, to within the expected accuracy of our approximations, in pretty good agreement with the observed perpendicular phase velocities:

$v_\perp \approx 480$ m/s (Argon)
$v_\perp \approx 690$ m/s (Helium)

Of course, the degree of shear of the (azimuthal) drift waves would affect the apparent radial phase velocity observed by our probes, but the above arguments suffice to indicate that more work must be done, and in particular the radial components of the electric field, and also of the density gradient, must be seperated from the azimuthal components. This will also allow us to determine the radial shear of the azimuthal waves, provided azimuthal waves are found to be present.

It is our tentative conclusion that both EIC and drift wave phenomena are present, and that mode conversion and/or some other non-linear interaction of these waves may be taking place. It is too great a coincidence to easily accept that we just happen to observe wave activity in the region of the intersection of the sets of fastest growing mode parameters for EIC waves and drift waves. In similar circumstances, waves and/ or instabilities with both drift and electrostatic ion cyclotron components interacting have been observed previously. Post and Rosenbluth, for example reported on the drift cyclotron loss-cone instability back in 1966, and Kando, Ikezawa, Sugai, and Kishimoto reported on ion cyclotron drift waves resulting from radial density gradients as recently as 1987. It is only speculation at this stage, but it seems likely at this stage that, in our experiments, drift waves may be growing up, saturating, and dumping their energy into EIC waves. This view is backed up by the observation, again from Schmidt, that for the fastest growing drift modes alluded to above, the growth rate is comparable to the real part of the frequency. This is very rapid growth. In our experiments, we see waves which grow up very quickly to a fairly stable amplitude. But while the amplitude may remain fairly constant overall, we do see evidence of strong steepening, and other non-linear features consistent with saturation. Yet if the waves are saturating, some other process must be removing energy from the waves, because the free energy source which provides the impetus for growth, the density gradient, is still present. It seems plausible at this stage of our investigation to suspect that EIC waves may be the mechanism by which energy is removed from the drift waves, and it may well be that they transfer the energy to the thermal electrons via Landau damping. If this is the case, then both EIC wave physics and drift wave physics would play roles in determining the structure of the transverse double lauyers we have observed.

After receiving the very useful suggestion from Dr. Chang that I consider the possible role of EIC waves, and after doing the analysis given above, I discussed my data and tentative conclusions with Dr. Hudson. I was particularly interested in obtaining her opinion as to the possibility that drift waves, and perhaps even drift wave-EIC wave interactions, might play a role in auroral processes. Her response was encouraging; she informed me that very sharp density gradients perpendicular to B exist in the auroral acceleration region, and in the source regions of auroral kilometric radiation. She mentioned that Persoon (JGR. '88) took langmuir probe data at about 1Re and found densities varying between one and a hundred per cc over a relatively short distance. Other evidence of this is provided by Poudellette (GRL.'87). All of this is encouraging in that it indicates that the coupling we appear to be observing in the laboratory may play a role in the auroral acceleration region as well.

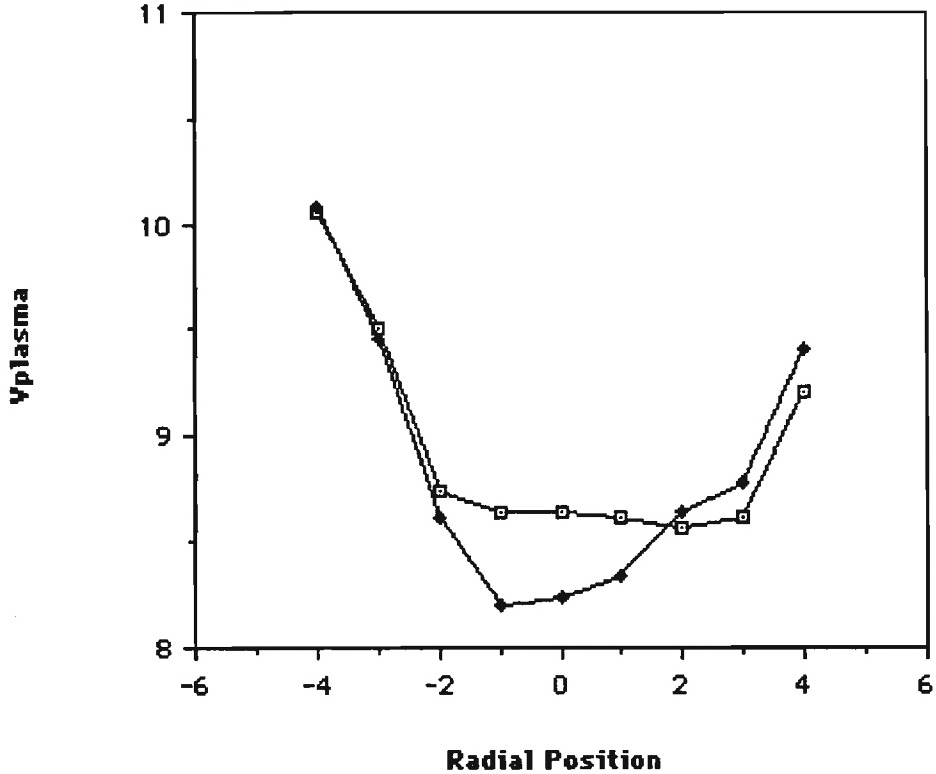

Plasma potential (in volts) as a function of radial position (in cm). Data was taken in an argon plasma. The hollow boxes indicate measurements taken with the south source only. The solid boxes indicate measurements taken with both the north and south sources operating. The probe is swept through the plasma on an arc of radius 6.35 cm. As these data were taken with the West probe, the negative radial positions are above and to the left side of the plasma axis, while the positive positions are below and to the right. In each case the magnitude of the radial position is the actual radius.

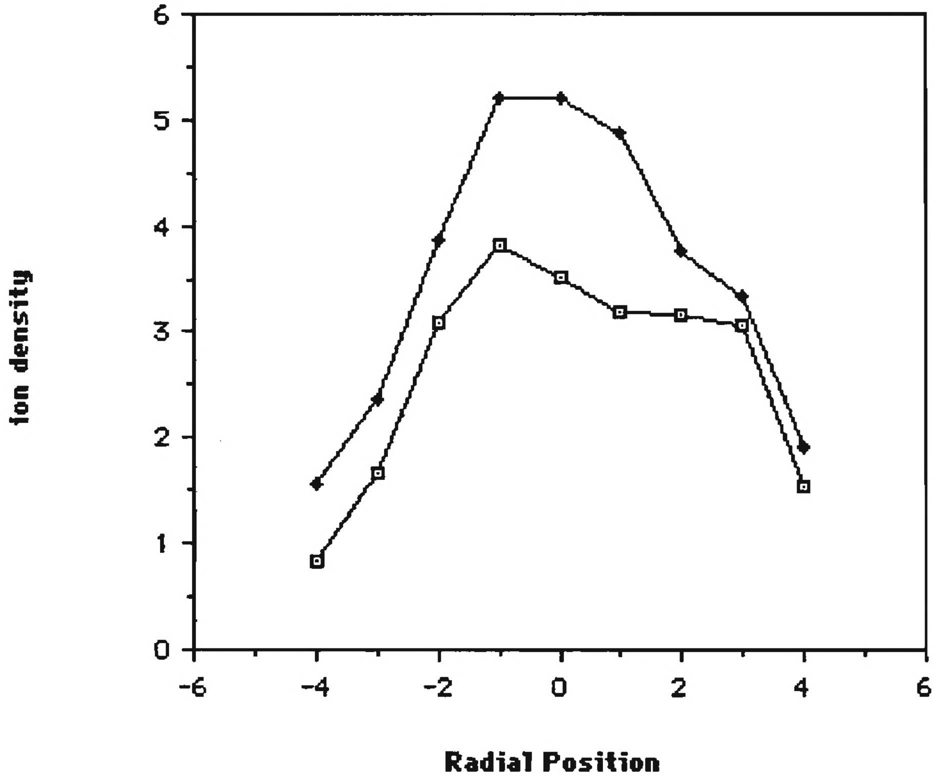

Ion density (in units of 10^9 cm^{-3}) as a function of radial position (in cm). Data was taken in an argon plasma. The hollow boxes indicate measurements taken with the south source only. The solid boxes indicate measurements taken with both the north and south sources operating. The probe is swept through the plasma on an arc of radius 6.35 cm. As these data were taken with the West probe, the negative radial positions are above and to the left side of the plasma axis, while the positive positions are below and to the right. In each case the magnitude of the radial position is the actual radius.

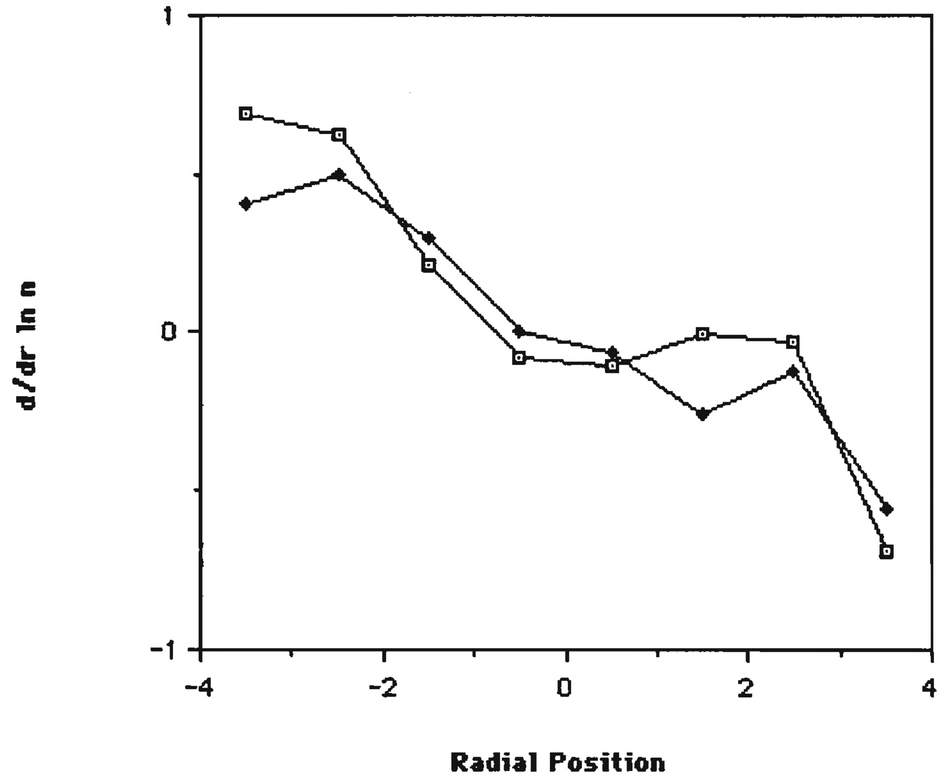

Derivitive of the logarithm of ion density with respect to radial position (in cm^{-1}) as a function of radial position (in cm). Data was taken in an argon plasma. The hollow boxes indicate measurements taken with the south source only. The solid boxes indicate measurements taken with both the north and south sources operating. The probe is swept through the plasma on an arc of radius 6.35 cm. As these data were taken with the West probe, the negative radial positions are above and to the left side of the plasma axis, while the positive positions are below and to the right. In each case the magnitude of the radial position is the actual radius.

Density and Electron Temperature Measurements

While our primary experiments involved collecting data on the transverse double layers observed during double plasma experiments, and in establishing upper bounds on the magnitudes of any axial potential jumps which might be present, it was also necessary for us to establish values for the important parameters characterizing the plasma, the temperature and the density.

Density profiles, and their changes with respect to time are, of course, part of the primary data on double layers, but as well as establishing the shapes and time variations of the profiles, it is necessary as well to establish an absolute calibration for the density. This is particularly true in a magnetized plasma, where particle collection techniques are notoriously difficult to directly interpret in absolute terms (see Hershkowitz). We calibrated our density measuring probe tips by comparing their ion saturation currents (at a range of voltages around -100V) with the resonance shift of a resonant cavity excited with microwaves well above both the plasma frequency and the electron cyclotron freqency; this is an established technique for measuring density in a magnetized plasma. This technique was repeated at a variety of plasma production powers, and a reasonably linear relationship between plasma density as determined by cavity resonance shift and probe ion saturation current was established. By linking the measurements from of our moveable ion collection probes to those from the well understood density measuring cavity (which is not moveable), we obtained a flexible probe system with good absolute calibration.

For our temperature measurement, we started with the well established technique of measuring the ion acoustic speed both in the upstream and downstream directions, but we modified it with a twist which we believe to be original (as well as effective), and which we intend to publish in Review of Scientific Instruments. There are a number of difficulties in successfully employing the ion acoustic method; one of the most pernicious problems is that to get a strong enough ion acoustic signal to deal with, it is frequently necessary to use use drive voltages which are comparable to or even larger than the electron temperature. This causes a sloshing of the electron population, which in turn affects the propagation speed of the ion acoustic waves much as if the electron temperature had been raised. Consequently, the standard version of this technique frequently gives electron temperatures which are higher than the actual values. The twist we have given this technique is that we launch our waves my modulating our plasma production power. Since we launch our ion acoustic waves by amplitude modulating the electron cyclotron resonant heating power of our plasma sources, we avoid the problem of axial electron sloshing, and obtain accurate electron temperature information. By modulating first one source, and then the other, we launch waves first up the tank, and then down it. By multiplying the drive frequency by the average of the upstream and downstream wavelengths, we obtain the ion acoustic speed with respect to the plasma (see following figures), from which electron temperature is easily determined. Measuring both upstream and downstream propagation speeds not only enables us to correct for the effects of plasma drift, but it also enables us to accurately determine what the value of that drift is. Thus the net plasma drift becomes yet another parameter over which we may exert control.

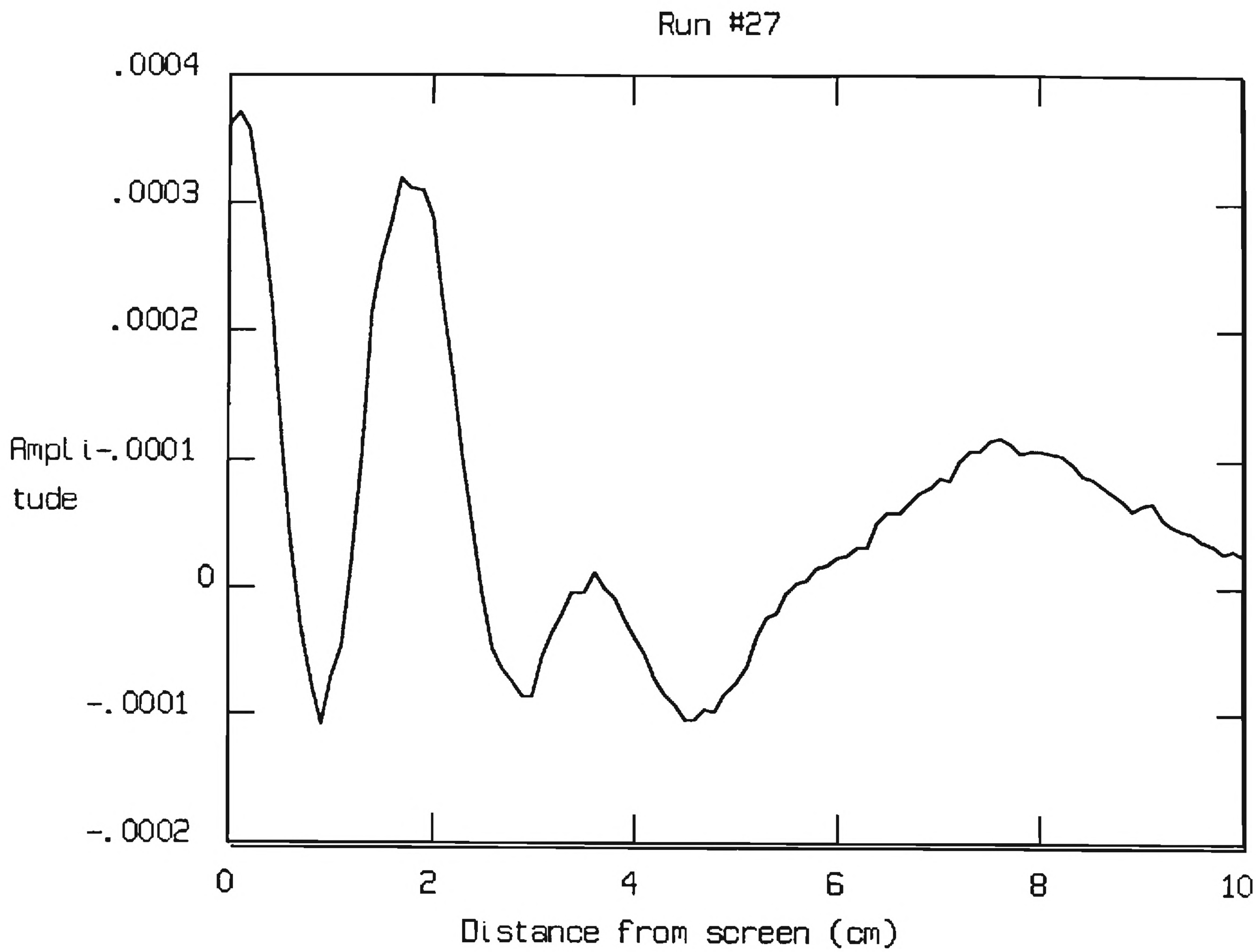

Run #27 Data Sheet
!date = 04/25/1989
!start time = 18:29:41
!Lock-In Reference frequency = 100000
!Can potential = gnd
!Middle screen potential = gnd
!Outer screen potential = gnd
!Anvil screen potential = gnd
!Copper plate potential = gnd
!FLUKE: freq. = 1497 MHz, power = 3.0 dBm, mod. = 25%
!Marconi: freq. = 747.5 MHz, power = -10 dBm, mod. = none%
!Probe angle = 0
!Gas = Argon
!Start Drift: (A-B)/(A+B-2*O) = -.157383 , A and B - Off= -1.1963 V
!End Drift: (A-B)/(A+B-2*O) = -.153416 , A and B - Off= -1.2022 V

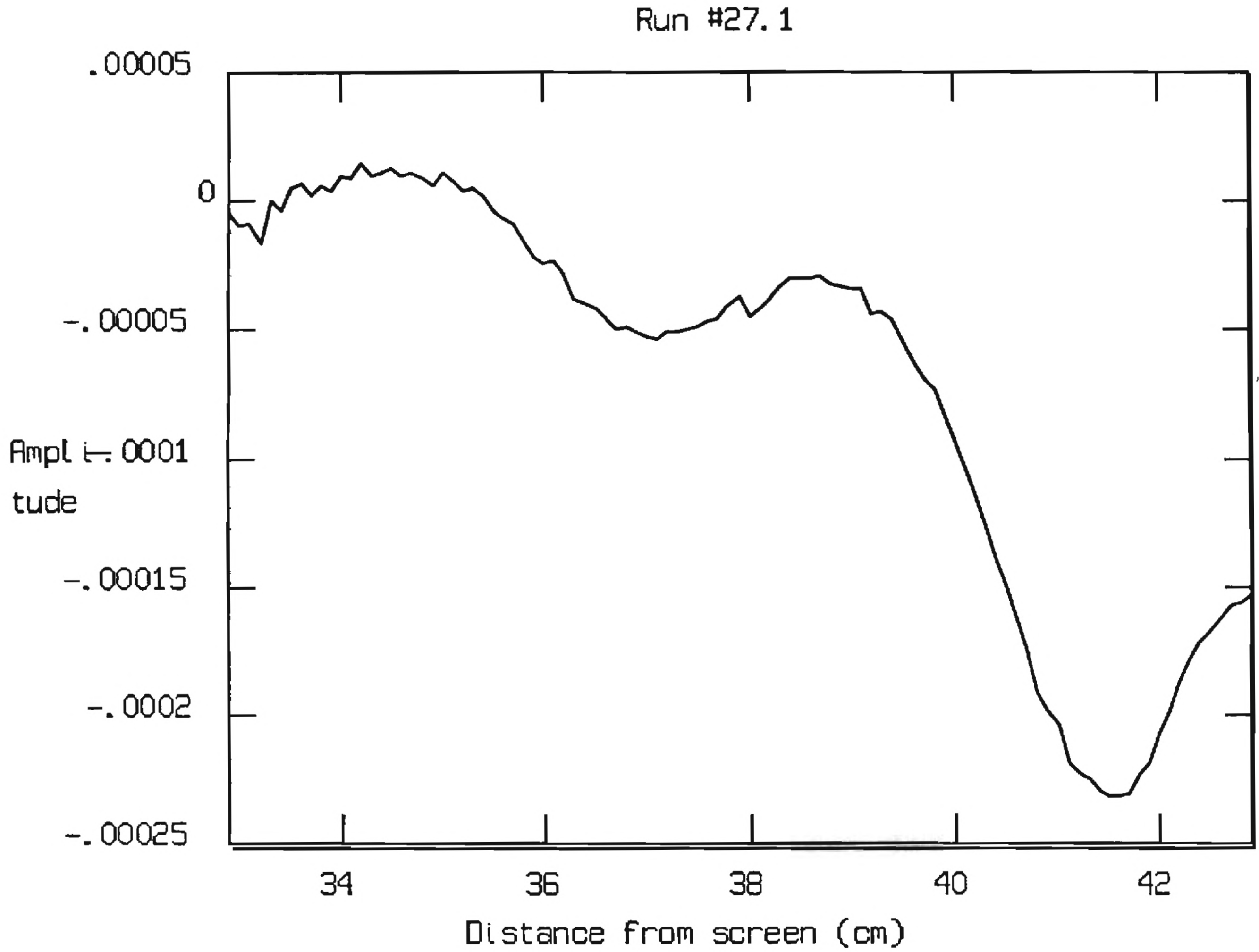

Run #27.1 Data Sheet
!date = 04/25/1989
!start time = 19:00:37
!Lock-In Reference frequency = 100000
!Can potential = 0
!Middle screen potential = 0
!Outer screen potential = 0
!Anvil screen potential = 0
!Copper plate potential = 0
!FLUKE: freq. = 1497 MHz, power = 3.0 dBm, mod. = none%
!Marconi: freq. = 747.5 MHz, power = -10 dBm, mod. = 25%
!Probe angle = 0
!Gas = Argon
!Start Drift: (A-B)/(A+B-2*O) = -.153369 , A and B - Off= -1.2606 V
!End Drift: (A-B)/(A+B-2*O) = -.125942 , A and B - Off= -1.2206 V

Computational Determination of Ion Temperature

The determination of the ion temperature in a plasma can be arrived at through the use of mathematical modeling using a computer. For instance, it its known that the rate of energy exchange between ions and electrons is governed by:

$$\frac{dT_\alpha}{dt} = \sum_\beta \bar{\nu}_\alpha^{\alpha/\beta} (T_\beta - T_\alpha)$$

where;

$$\bar{\nu}_\alpha^{\alpha/\beta} = 1.8*10^{-19} \frac{(m_\alpha - m_\beta)^{1/2} Z_\alpha^2 Z_\beta^2 n_\beta \lambda_{\beta\alpha}}{(m_\alpha T_\beta + m_\beta T_\alpha)^{3/2}}$$

and;

$$\lambda_{\alpha\beta} = 23 - \ln (n_e^{1/2} Z T_e^{-3/2})$$

Through the knowledge of our electron temperature a True Basic program was written to solve for the ion temperature. All formulas were taken from D. L. Book, NRL Plasma Formulary, 1987.

Data Narrative

The following data plates are numbered to facilitate communication, but a few code word explanations should suffice to explain much straight out. KS or Kemp Sellen or V_p refer to plasma potential measurements taken with an emitting probe. Ion sat or Langmuir probe or LP refer to ion density measurements. In most (but not all) cases, only fluctuating quantities are shown; the dc values are considerably greater in general, and are represented on separate graphs which are also included. Plate 4 shows both fluctuating ion density, and a zero reference on the same graph. The magnitude of the KS fluctuations may be directly read in volts, and I will be glad to convert any of the ion sat plates from volts to cm^{-3}, if desired. Please note that the **time per division** is indicated in the lower right hand corner, and also in the box by each trace. When different times per division are indicated on the same plate, the values in the boxes must be observed. In the case of averaged quantities, the boxes will also indicate what is being averaged; ie. <1> 200 indicates that channel one has been averaged 200 times, and the result displayed. Hammer refers to the North source, which is pulsed and whose onset is indicated by the arrow on the bottom of the graph. Anvil refers to the South source, which is always on in these shots. The original plates are in color, which helps me to distinguish between multiple traces, and I will be glad to answer questions in cases of confusion as to the identity of traces on multiple trace plates.

Many of the structures represented on these plates appear strongly non-linear, and most survive, at least in part, over many averages, indicating that the waves which grow up in response to the hammer fall have a significant part which is not stochastic.

Plates 9 through 12 show a very interesting sequence of shots. In each of these, Memory D is displaying the same graph of a single shot of plasma potential versus time, while other single shots are shown for comparison in plates 9 throuth 11, and a 200 shot average is displayed in 12. Note that there is a delay of about 25 μs, after which a string of solitary waves of width about 25 μs begins. That this is a string of solitary waves, and not just an ordinary wavelike oscillation is evidenced by the fact that the solitary waves may appear in a train, as in Mem D on all the plates, or singly as in plate 10, in pairs, as in plate 9, or even as an otherwise complete train with one tooth missing, as in plate 11.

The plates from 20 on serve to show how little difference is made in the arrival time of the observed structures by a large (23 cm) axial seperation between probes. On the other hand, as little a radial difference as 1 cm results in an easily observable shift in arrival time.

Note that in some of the plates, particularly in the less interesting plates (ie. those in which only gentle fluctuations, without steepening, are noted) the fluctuations in the ion density are mirror images of fluctuations in the plasma potential when the probes have a similar transverse location. This is characteristic of Drift waves (see Marden Marshal and Hall). This relationship appears not to depend on the relative axial location of the probes. Similarly, when both probes are used in ion saturation, the signals obtained are identical, to within the noise level (which is fairly low), provided that the transverse location of the probes is the same. Furthermore, even for the more interesting plates, for which the relationship between the ion density and plasma potential signals will generally be much more complicated, the difference between traces can be seen to be a continuous functiuon of the transverse separation between the probes, and that this function is monotically increasing with probe separation up to transverse separations of about 4cm. Again, this is all independent of the axial separation. For cases where both probes measure ion saturation, the signals between probes at the same transverse location are essentially identical, for both the interesting and mundane cases. Yet again, all accessible axial location appear to produce indistinguishable results.

Plate designation #28 is the last of the first collection; this is followed by a shorter second collection from run #37, whose members bear the designations 51 to 57.This collection of shots shows some of the variety which may be obtained by looking at the same probes on different hammer pulses, but otherwise under very similar conditions. This collection consists of plates taken during a single run, and I have rearranged them to provide an increasing level of dissimilarity between the ion density and plasma potential traces. At the beginning of this collection we have fairly uninteresting shots which appear to show nothing but drift waves. As we progress through the collection, the East probe (which is of the Kemp-Sellen type, which measures plasma potential) begins to demonstrate more and more independence. In the third to last and second to last plates in this sequence, #55 & #56, the Kemp-Sellen probe shows respectively, a single peak, and a pair of peaks. Note that the ion density traces show little, if any, sign of this string of peaks which is so evident on the plasma potential traces. The last trace in this collection, #57, shows detail of a higher frequency wave which showed up on the plasma potential trace alone. Note that the record of the scope settings show that, in this last trace, time per division was expanded and sensitivity increased. This collection of plates strongly suggest that we have drift wave activity as a result of the universal density gradient instability during our normal operation, and that this activity is giving rise to some other type of acitvity with a different relationship between ion density and plasma potential fluctuations (because of the similarity of $k_\perp$ values for nearly transverse EIC waves and drift waves at the observed frequencies, mode conversion between the two is a distinct possibility).

In run #40, plates #101 to #104, we see a situation where there is much more of a direct correlation than the inverse corellation noted above (and ascribed to drift waves). The major difference here is that the data discussed above were taken near the center of the plasma column, while Run #40 explored plasma behavior in the edge regions. Plate 40;23, ie. #101, is taken with the ion saturation probe near the bottom of the plasma column, and the plasma potential probe a centimenter closer to the center of the column (and more or less above the other probe). This plate shows some positive corelation between ion saturation and plasma potential. The other three these plates represent data taken with both probes near the bottom of the plasma column; here the corelation between the two signals is much stronger. In this configuration the probes overlap for about a centimeter, and thus are not precisely at the same transverse location, but they are sufficeintly close to show us not only <u>direct</u> corelations between plasma potential fluctuations and ion density fluctuations (as opposed to the inverse corelations noted above in data taken near the center of the plasma column), but also some very interesting potential and density structures.

The first of these three plates, plate 40;25, #102, shows simultaneous abrupt drops in both the plasma potential (magnitude about 3V) and the ion density at about 550 μs after the initiation of the hammer pulse (the event at 800 μs should be ignored; it is merely the termination of the hammer pulse, which of course has a dramatic prompt effect on both density and plasma potential diagnostics). Plate 40;26, #103, shows a somewhat less abrupt drop in the ion saturation signal at the same time as 40;25, but in this case the drop in the in the plasma potential is delayed to around 600 μs, and is somewhat larger than before (a little over 4V). Plate 40;29, #104, tells a somewhat different story; in this case the poential and ion density drops begin at about 550 μs, as before, but both recover to about their original values by about 600 μs. Thus the structure shown in 40;29 apears to be more of a soliton than a double layer. Note that both sensitivities have been changed between 40;25 and 40;29, and the potential trough is about 2.4V deep. This structure is reminescent of the theoretical work on ion holes done by Berman, Tetreault, and DuPree (see Ref.), and may represent such a structure in our strongly magnetized plasma.

A group of shots showing a dramatic string of peaks is displayed in the plates labeled 9 - 12,back in the first collection, but in this group the corresponding ion density variation is not displayed. This group suggests strongly that the string of peaks do not constitute a single linear wave, but rather constitute a string of solitary waves. As well as the comparison trace consisting of five peaks which is displayed on all of the plates 9-12, plate 10 displays a trace with a single peak, plate 9 displays a pair of consecutive peaks, and most telling of all, plate 11 displays a trace which has all of the expected peaks except the second, which is completely absent. Note that the spacing of the peaks is so nearly constant that the 200 shot average displayed on plate 12 shows a very coherent averaged signal. The signals in this sequence may well correspond to the lobes of a drift instability distorted plasma column whipping by, and the unusual strings might correspond to malformed fluted plasma columns. These plates were taken in a parameter regime where we intentionally accentuated our radial density gradient far above normal values, and these waves are almost certainly an exagerated version of drift waves.

Last is presented a short third collection (partially redundant with the first), which is labeled in a self-explanatory way, for convenience, rather than being renumbered.

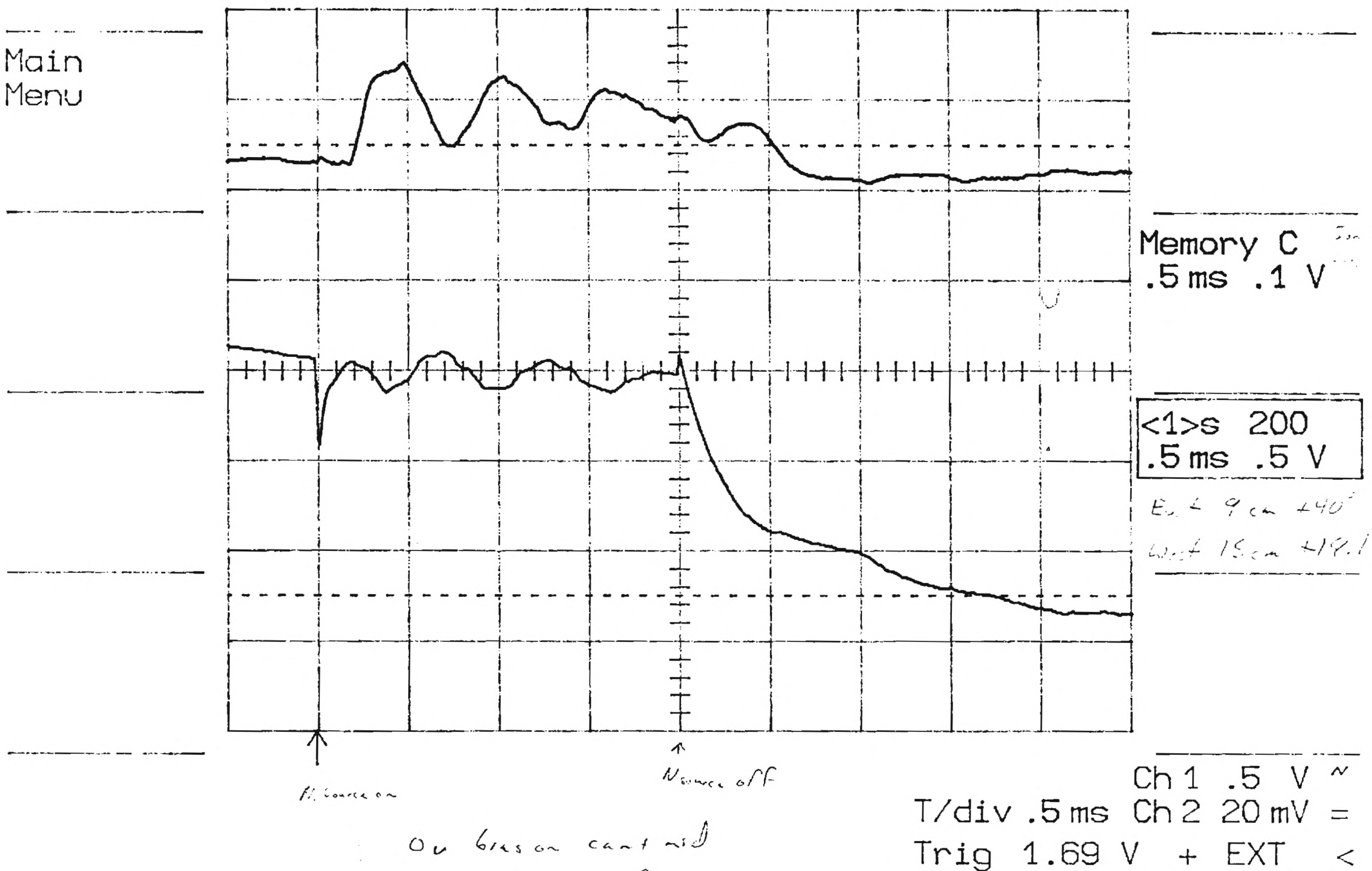

On bias on cont mid
.36 mA current from
control to gnd

Main
Menu

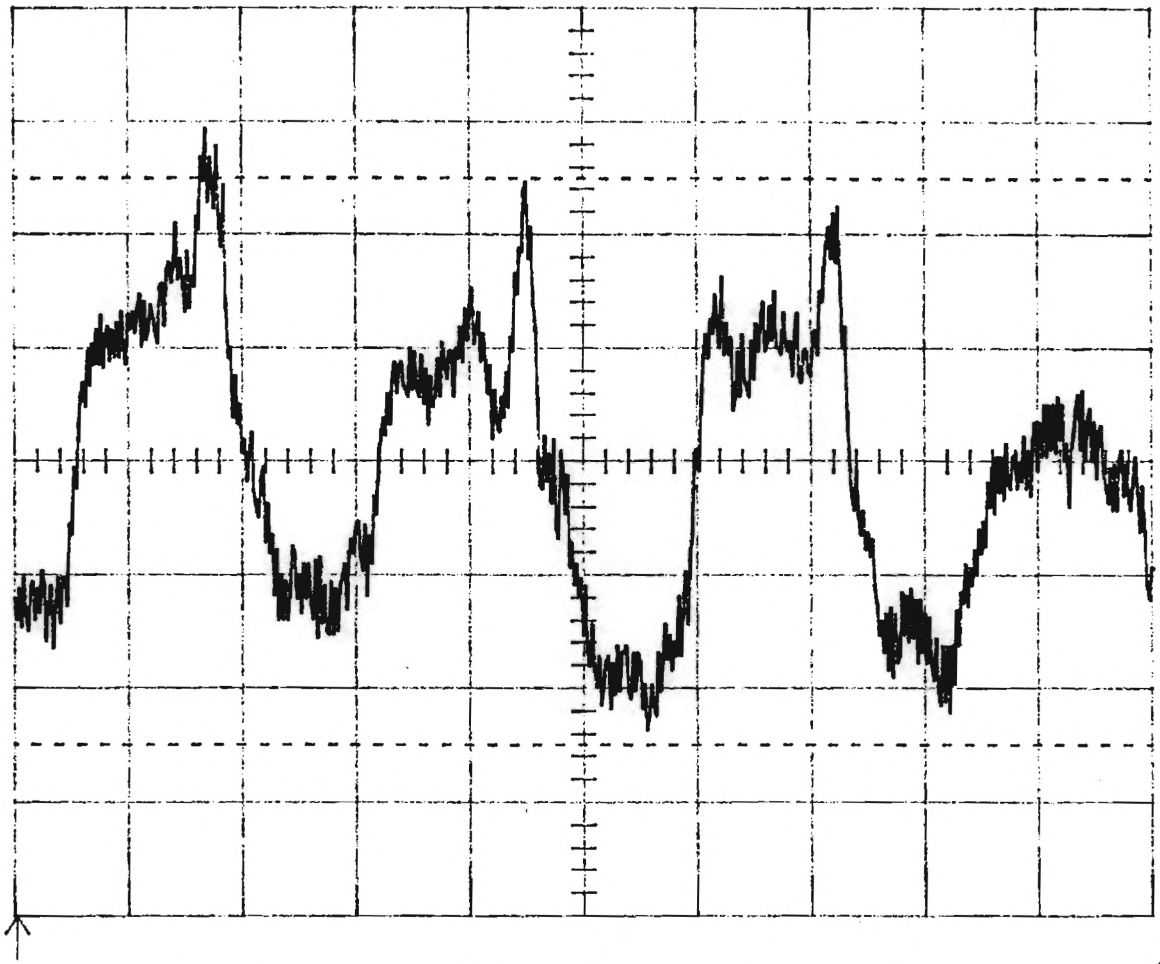

Channel 1
.2 ms .2 V

West
KS
15 cm =
18.1°

Hammer on continuously

0V can + mid

.60 mA can → gnd

Ch 1 .2 V ~
T/div .2 ms Ch 2 20 mV =
Trig 1.69 V + EXT <

Main
Menu

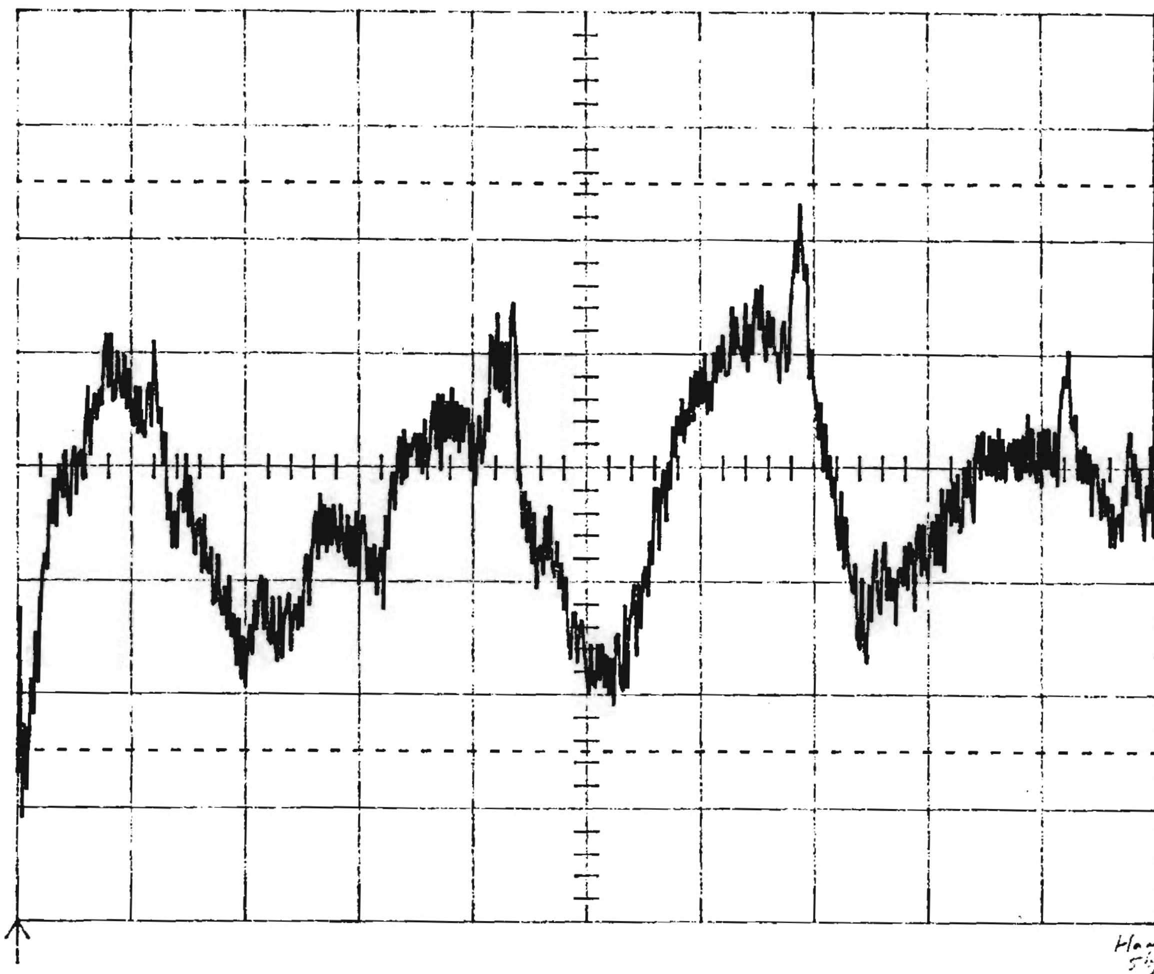

Channel 1
.2 ms .2 V

Hammer
Ch 1 .2 V ~
T/div .2 ms Ch 2 20 mV =
Trig 1.69 V + EXT <

0V cant mid
.35mA cant gnd

Main
Menu

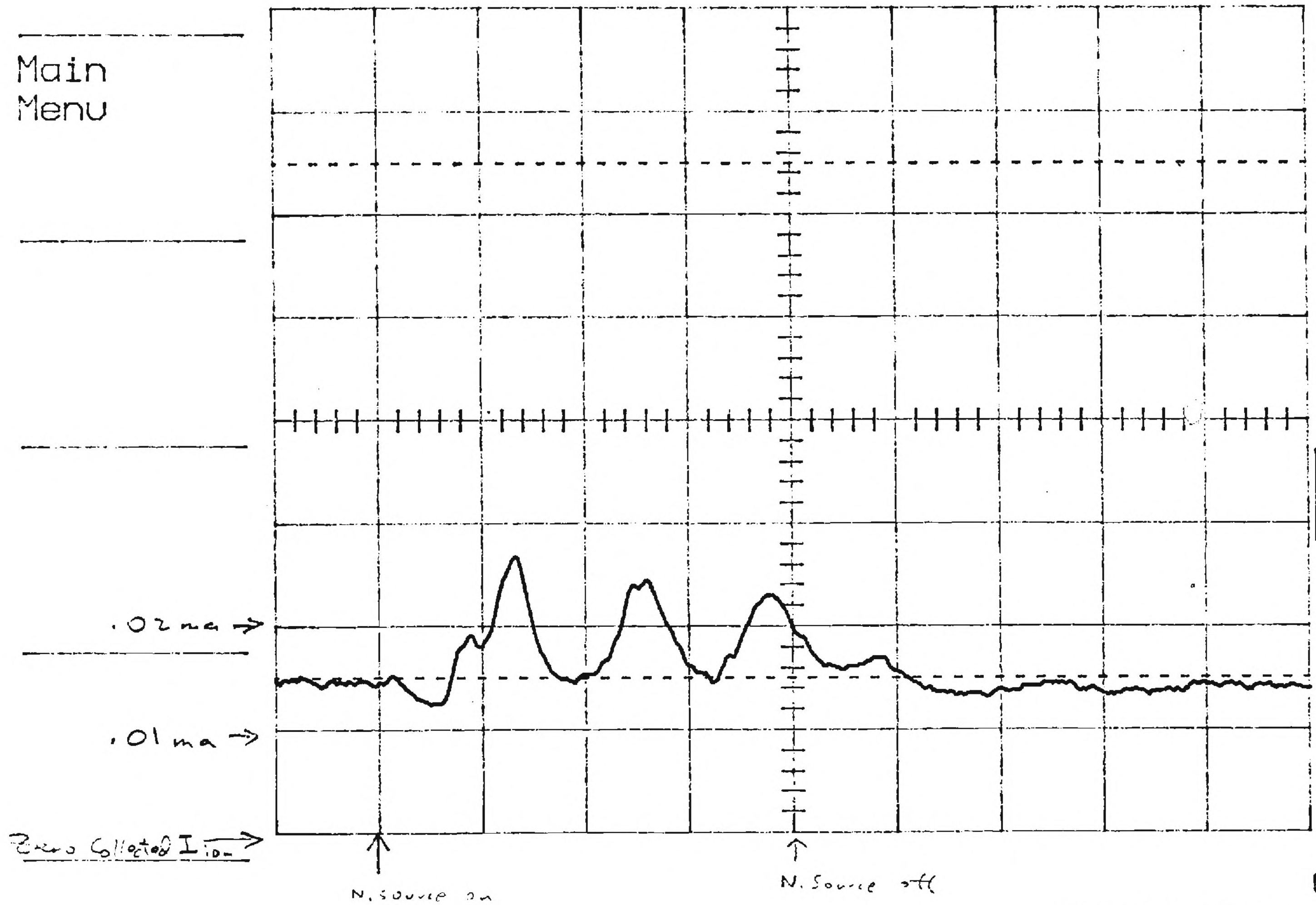

<1>s 200
.5 ms .1 V

West probe
1500 ⇒ 15 cm
r = +4 cm
Ion Saturation
-95.2 mA
10 kΩ

0 v bias on can + mid
.37 ma current from
Can + mid to gnd.

Ch 1 .1 V =
T/div .5 ms Ch 2 20 mV =
Trig 1.69 V + EXT <

4

Argon

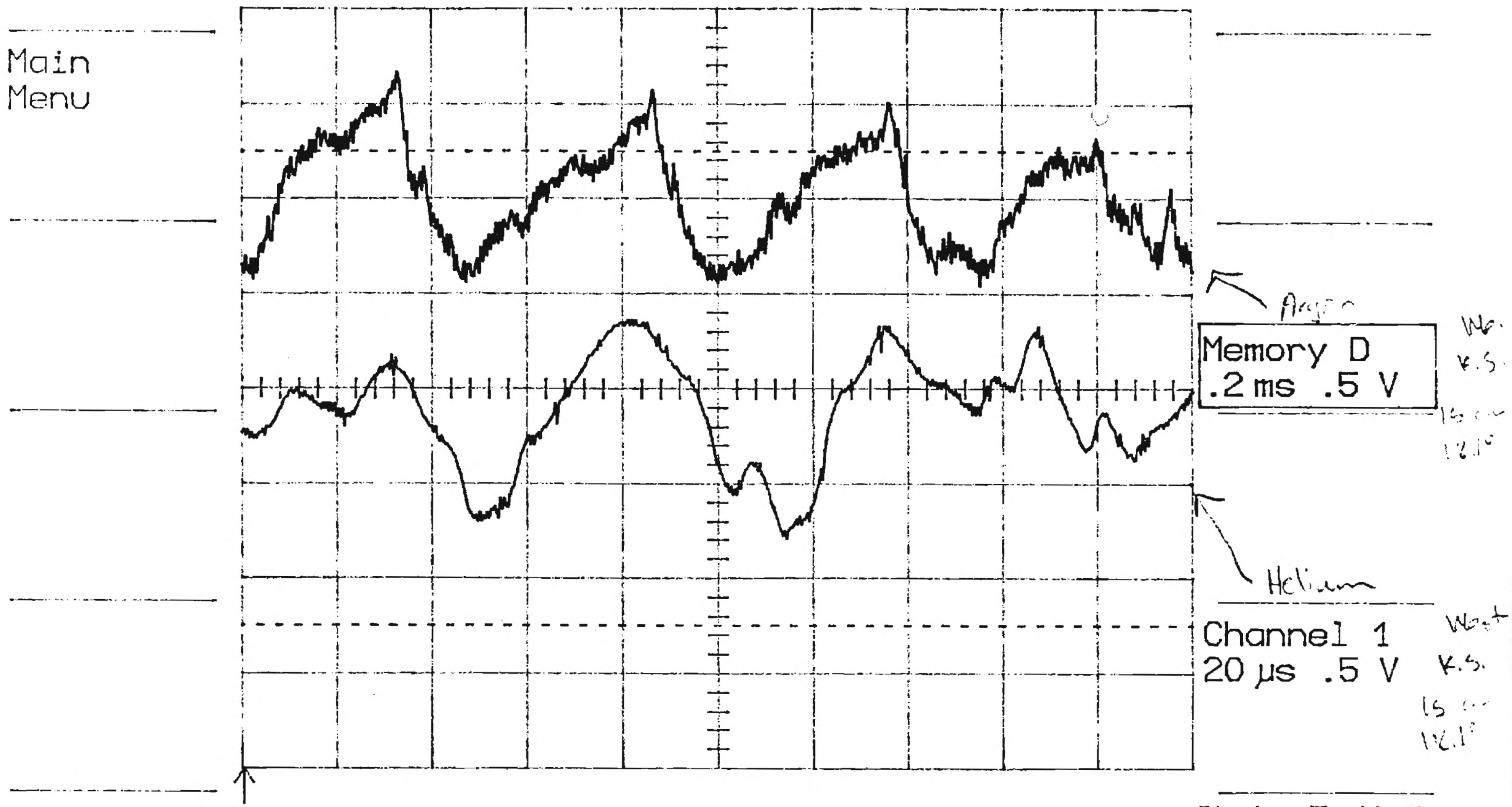

Ch 1 .5 V ~
T/div 20 µs Ch 2 20 mV =
Trig 1.69 V + EXT <

0 V cam + mid

Argon Trace = .846 V ±.01 cap mon.

Main
Menu

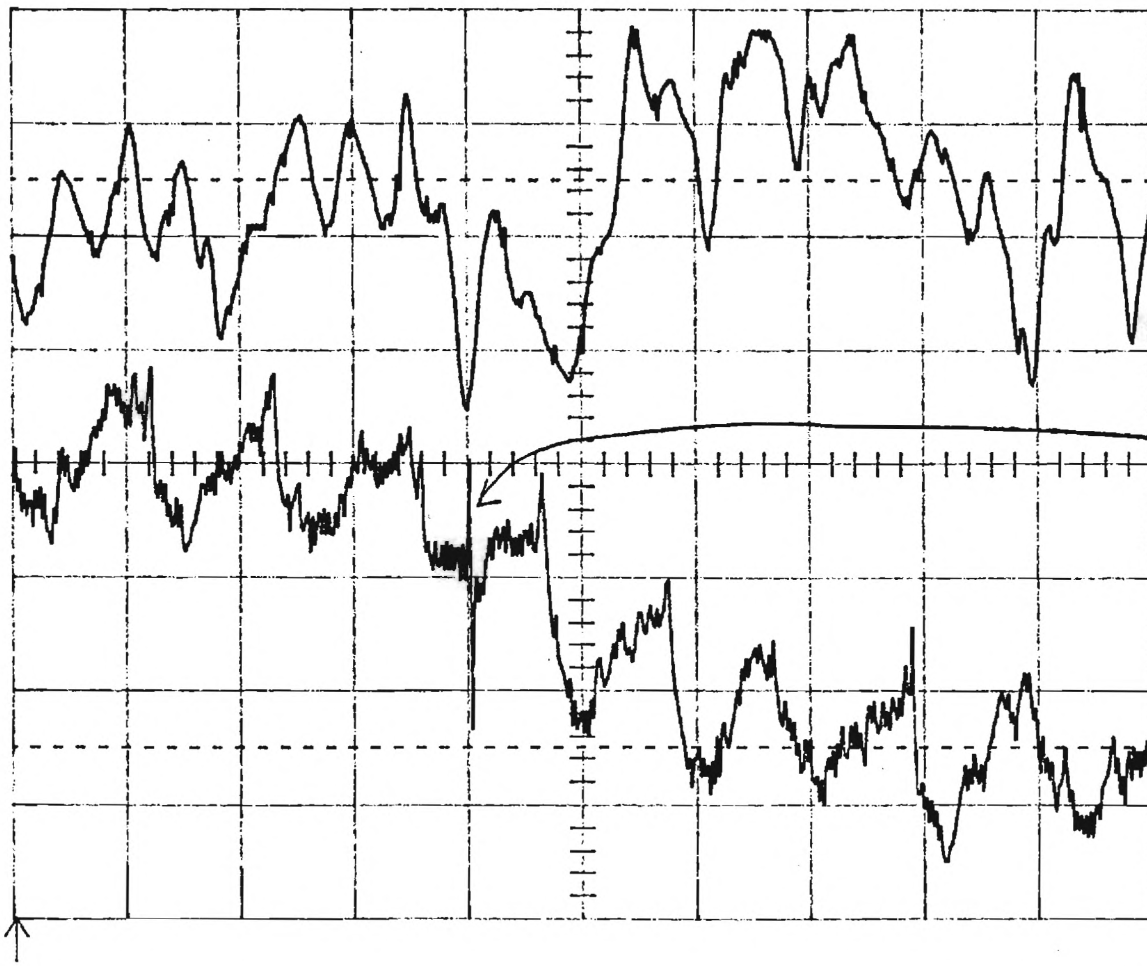

← Helium

Memory C
50 µs .5 V

West
K S.
15 cm
18.1°

end of heating pulse glitch (.5 ms scale only)

← Argon

Channel 1
.5 ms .5 V

West
K. S.
15 cm
15.1°

Ch 1 .5 V ~
T/div .5 ms Ch 2 20 mV =
Trig 1.69 V + EXT <

0 V cent mid

6

Main
Menu

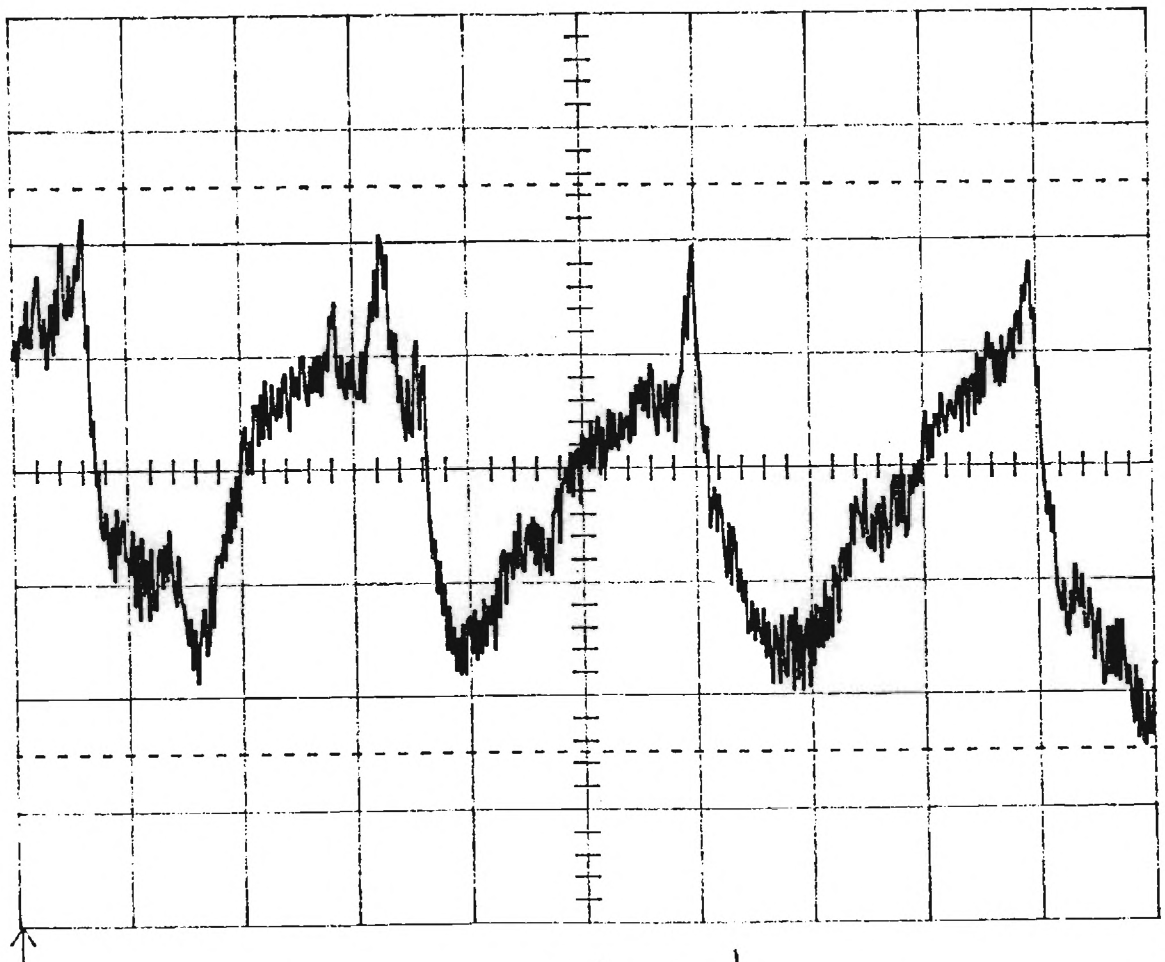

Channel 1
.2 ms .2 V

Wrist
KS
15 cm = 150
14.1° = +2c

Ch 1 .2 V ~
T/div .2 ms Ch 2 20 mV =
Trig 1.69 V + EXT <

Hammer on continuously
(not pulsed)

0 V can + mid
~.62 mA can → gnd

7

..., and [illegible], otherwise
(synchronized)

st as # 7.

On bias [illegible]

4.02 mA current flow [illegible]

Z=15cm

Main
Menu

~~5.21 kHz~~

[illegible] speed : 692 m/s ~~[illegible]~~

$\lambda_\perp = .0265\,m = \cancel{2.65\,cm}$ 2.61cm

$k_\perp = 237\,m^{-1}$

$.78 \times 10^{-5}$ sec
$= 2.65 \times 10^{4}$ Hz

$= \lambda_\perp = 2.61 \times 10^{-2}$

$= k_\perp = 241\,m^{-1}$

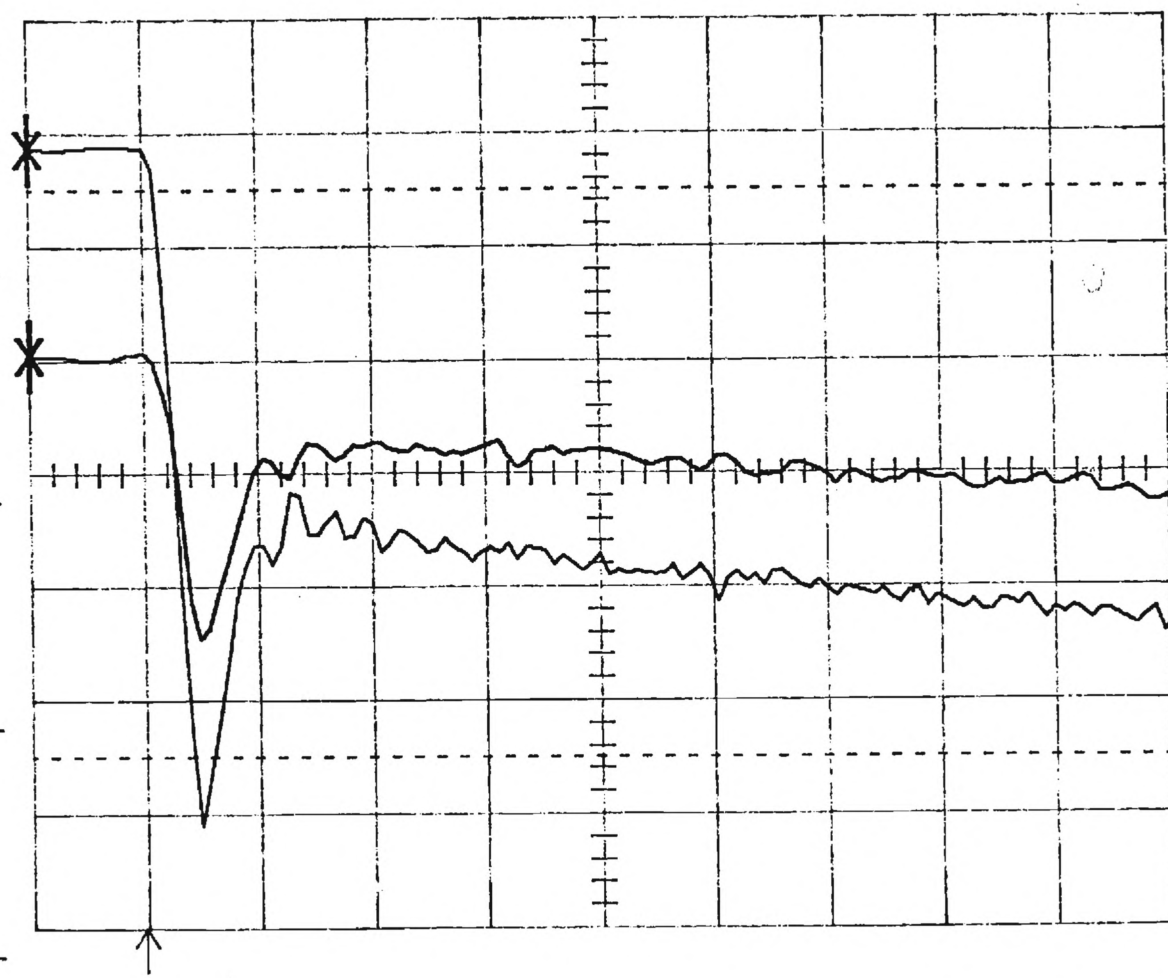

r = -3cm

r = -2cm

X-Mem D
.0 mV .1ms .5V

X-<1>s 200
.0 mV .1ms .5V

Ch 1 .5 V ~
T/div .5 ms Ch 2 20 mV =
BWL Trig 1.72 V + EXT <

Δt 0 ns f ∞

(S

(can emit (-8.04V)
-.03 mA current flow)

K-5 #1
2.15 m

6-Jun-89
20:01:49

LeCroy

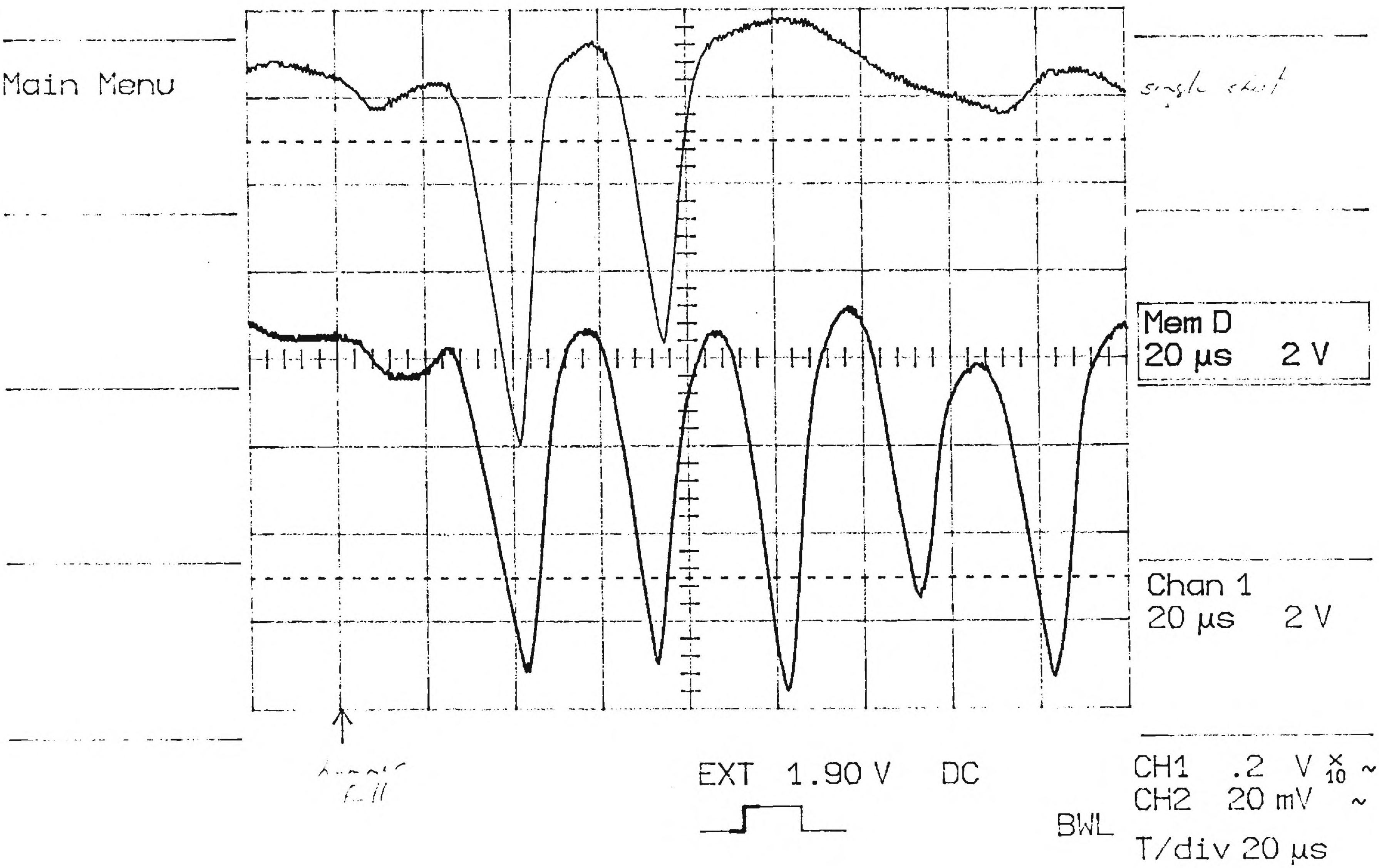

9

(can e mil @ (-8.04V))
(-.07mA current flow)

6-Jun-89
19:57:39

LeCroy

Main Menu

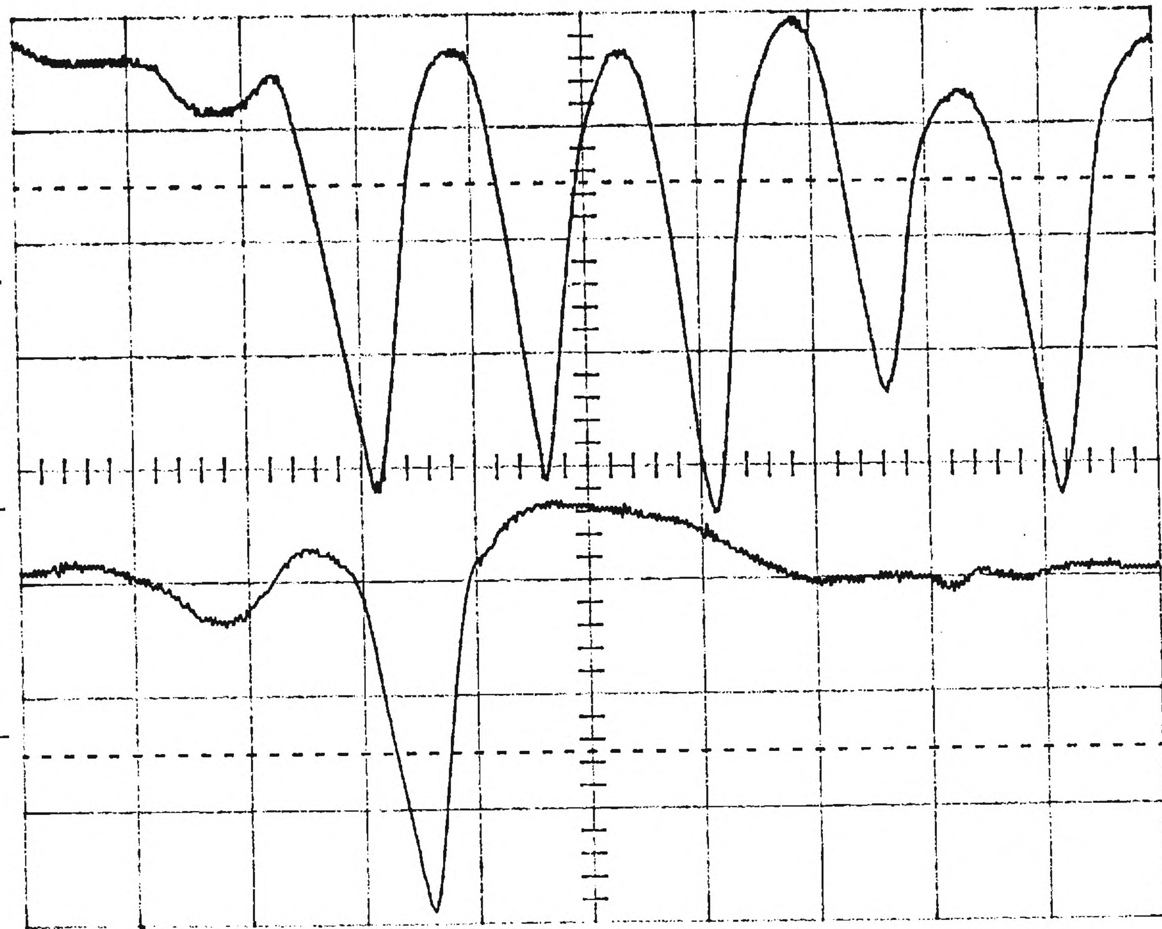

single shot

Mem D
20 µs 2 V

single shot

Chan 1
20 µs 2 V

hammer fall

EXT 1.90 V DC

BWL

CH1 .2 V x10 ~
CH2 20 mV ~
T/div 20 µs

Canemid @ (-8.04V)
(-.08mA current flow)

K-S T/p
2.15cm
r=2.m

(of 49.20)

6-Jun-89
19:48:12

LeCroy

Main Menu

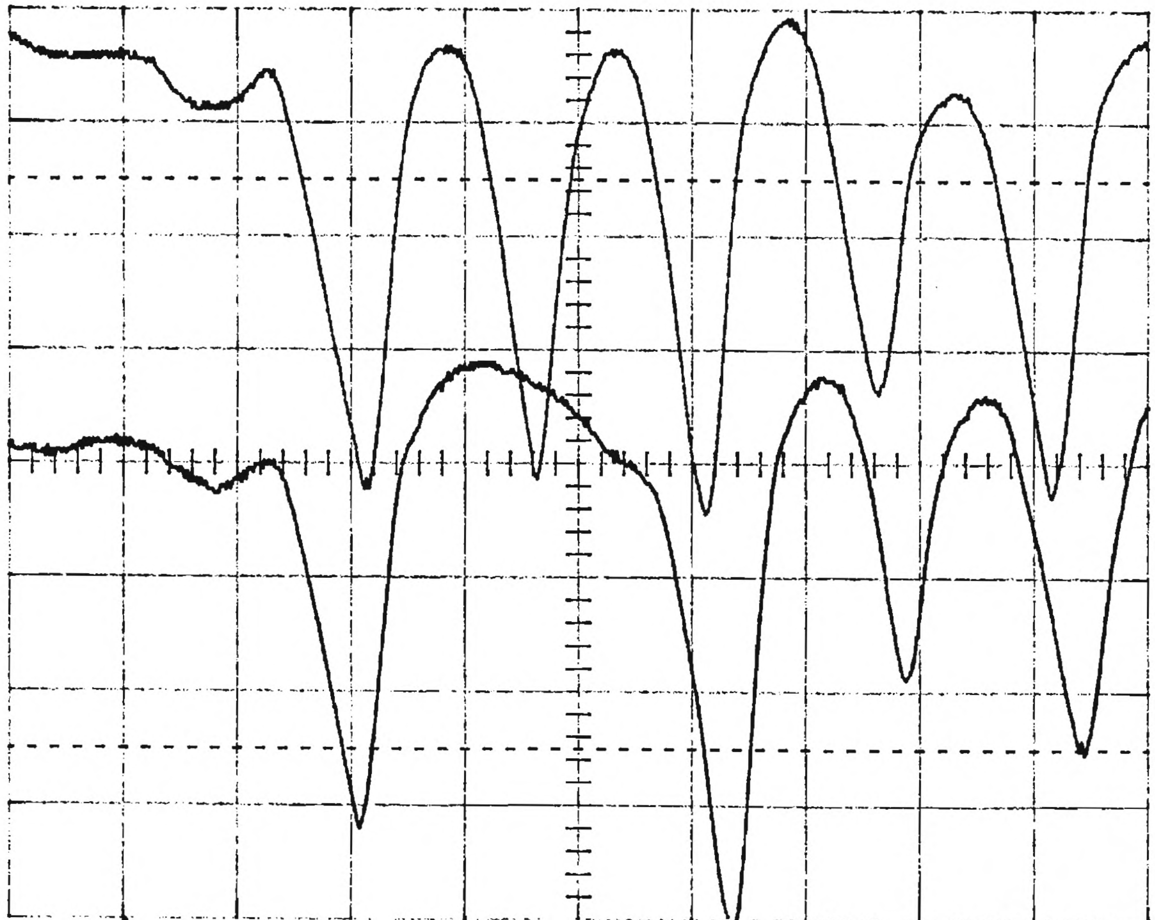

single shot

Mem C
20 µs 2 V

Mem D
20 µs 2 V

EXT 1.90 V DC

BWL

CH1 .2 V x10 ~
CH2 20 mV ~
T/div 20 µs

11

Can x mid @ (-8.04V)
(-.09mA current flow)

z=15cm
r=0

6-Jun-89
19:53:58

LeCroy

Main Menu

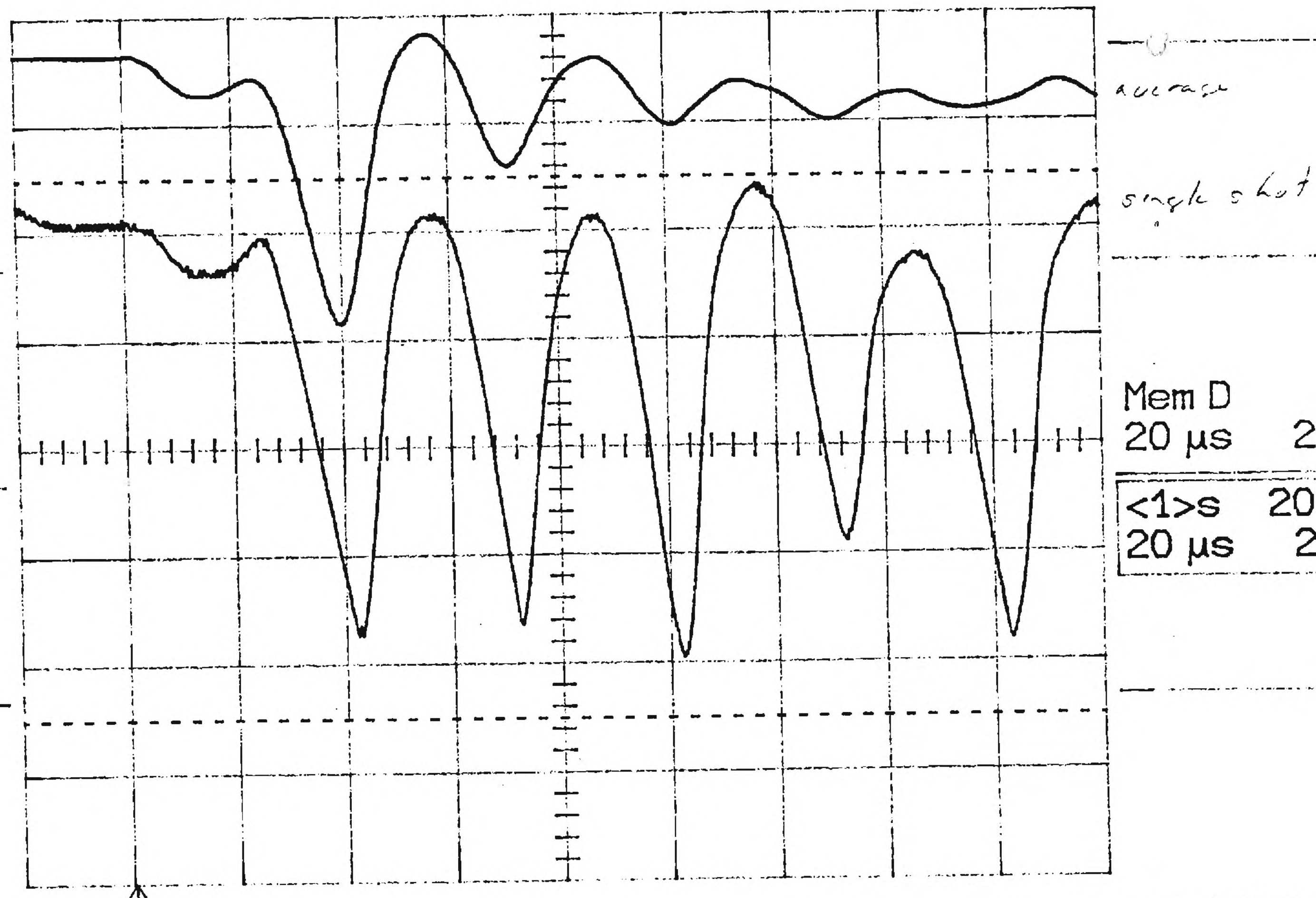

EXT 1.90 V DC

BWL

CH1 .2 V x10 ~
CH2 20 mV ~
T/div 20 µs

12

z=15cm
r=-4cm

case & mid tied together & ~~floating~~ 0V bias
+.12 mA current flow (with hammer off)

6-Jun-89
17:36:16

LeCroy

Main Menu

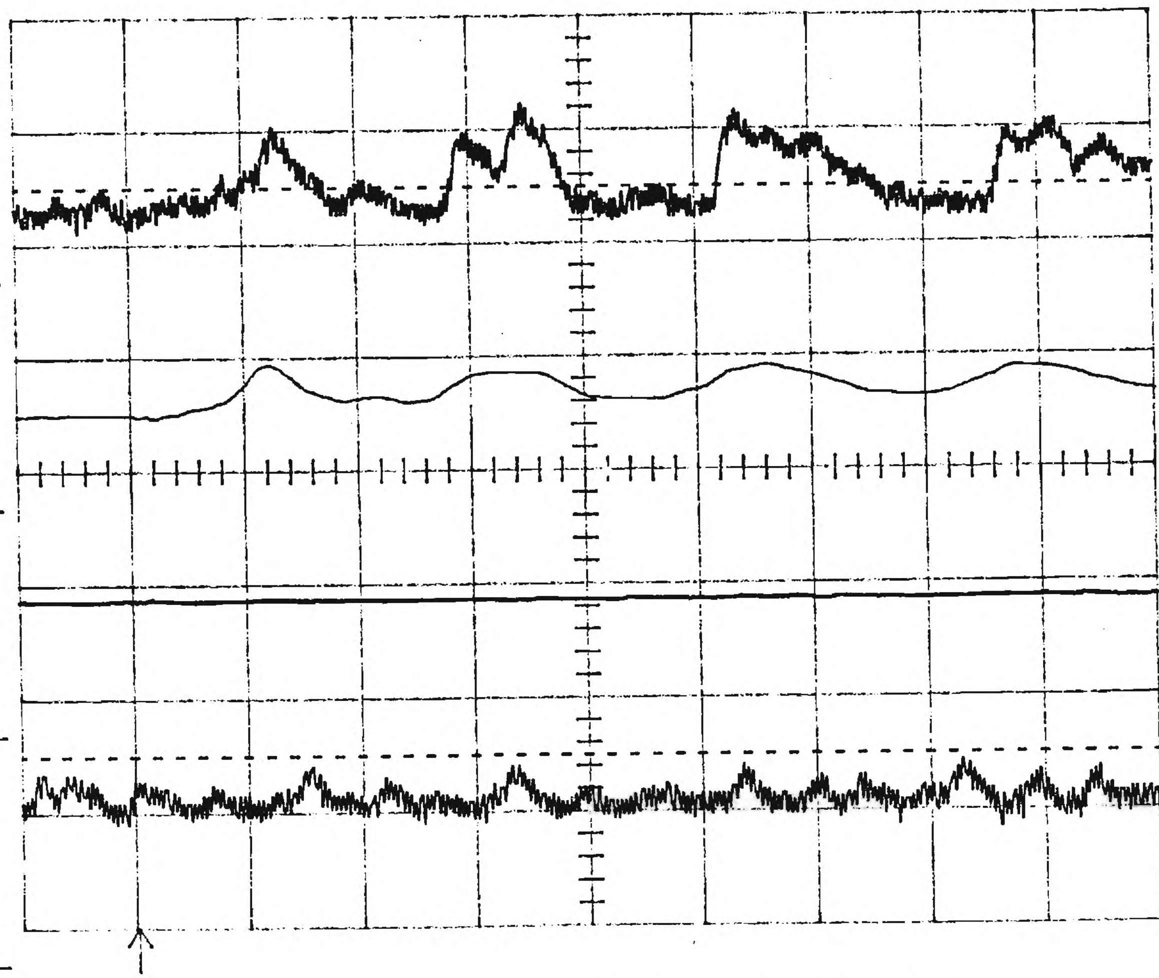

single shot with hammer

Mem C
.2 ms .2 V
averaged shot with hammer

Mem D
.2 ms .2 V

average - no hammer

<2>s 200
.2 ms .2 V

single shot - no hammer

Chan 2
.2 ms .2 V

hammer on

EXT 1.90 V DC

CH1 50 mV x10 ~
CH2 .2 V ~

T/div .2 ms

13

Can & mid tied together & ~~floating~~ 0V bias, 30 mA current flow

z = 15 cm

6-Jun-89
17:29:52

LeCroy

Main Menu

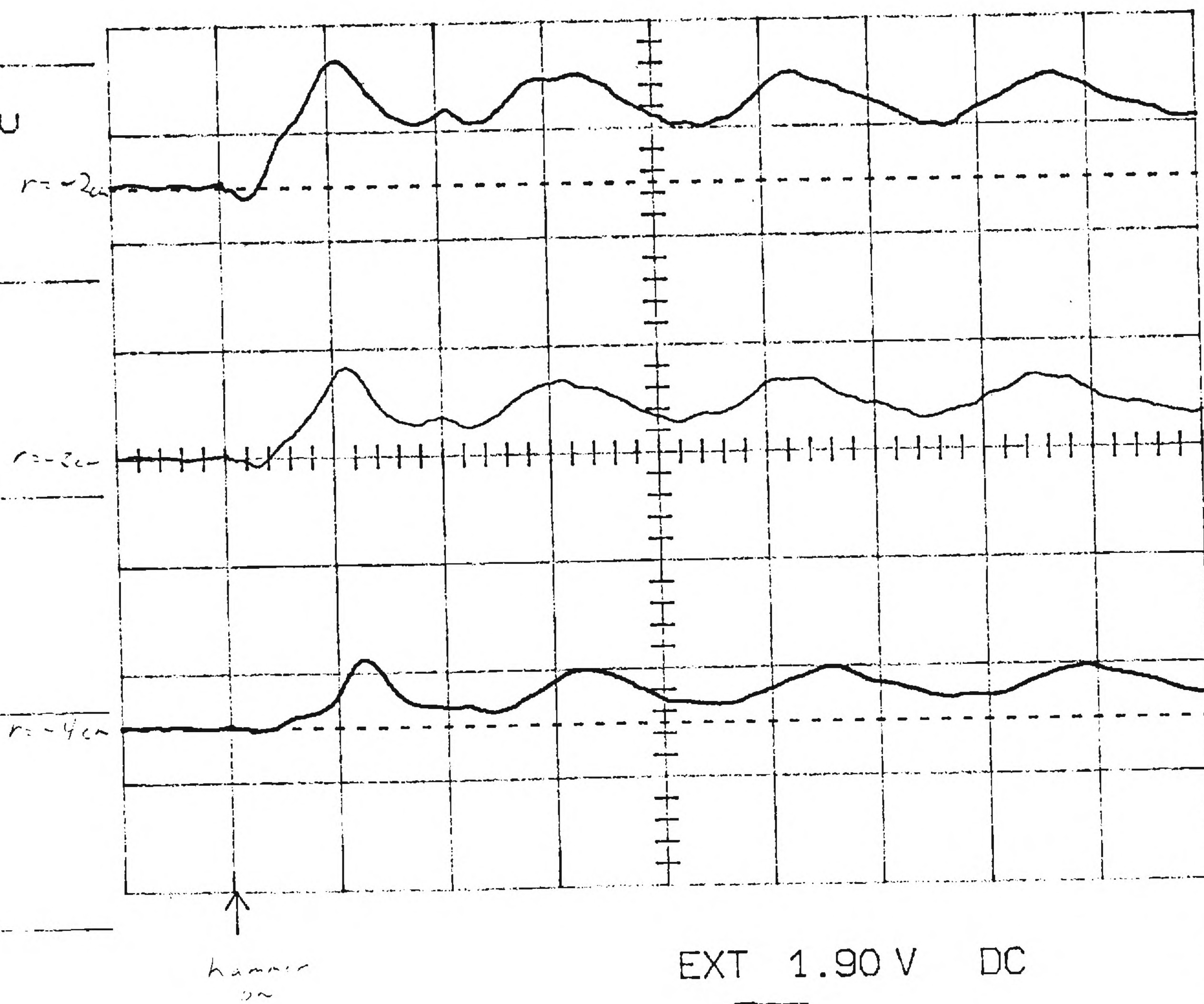

Mem C
.2 ms .2 V

Mem D
.2 ms .2 V

<2>s 200
.2 ms .2 V

EXT 1.90 V DC

CH1 50 mV x10 ~
CH2 .2 V ~

T/div .2 ms

6/6/89

Can emit tied together & ~~floating~~ 0 v bias
.30 mA current

6-Jun-89
17:23:18

LeCroy

Main Menu

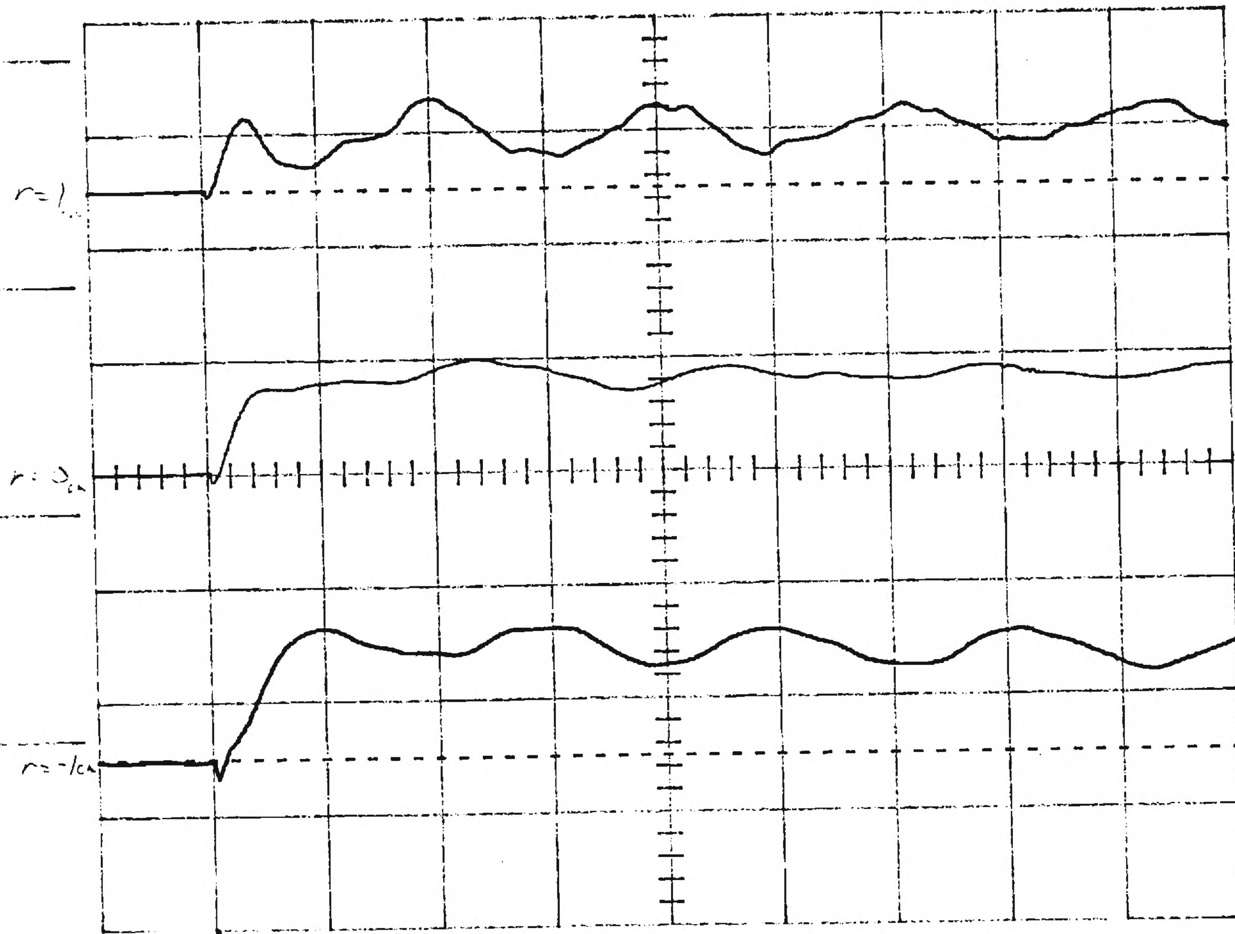

r=1cm

Mem C
.2 ms .2 V

Mem D
.2 ms .2 V

r=0cm

<2>s 200
.2 ms .2 V

r=1cm

EXT 1.90 V DC

CH1 50 mV x10 ~
CH2 .2 V ~

T/div .2 ms

can + mid tied together & ~~floating~~ 0 V bias
.30 mA current

ion sat
z = 15cm

6-Jun-89
17:15:46

LeCroy

Main Menu

r = 4cm

r = 3cm

r = 2cm

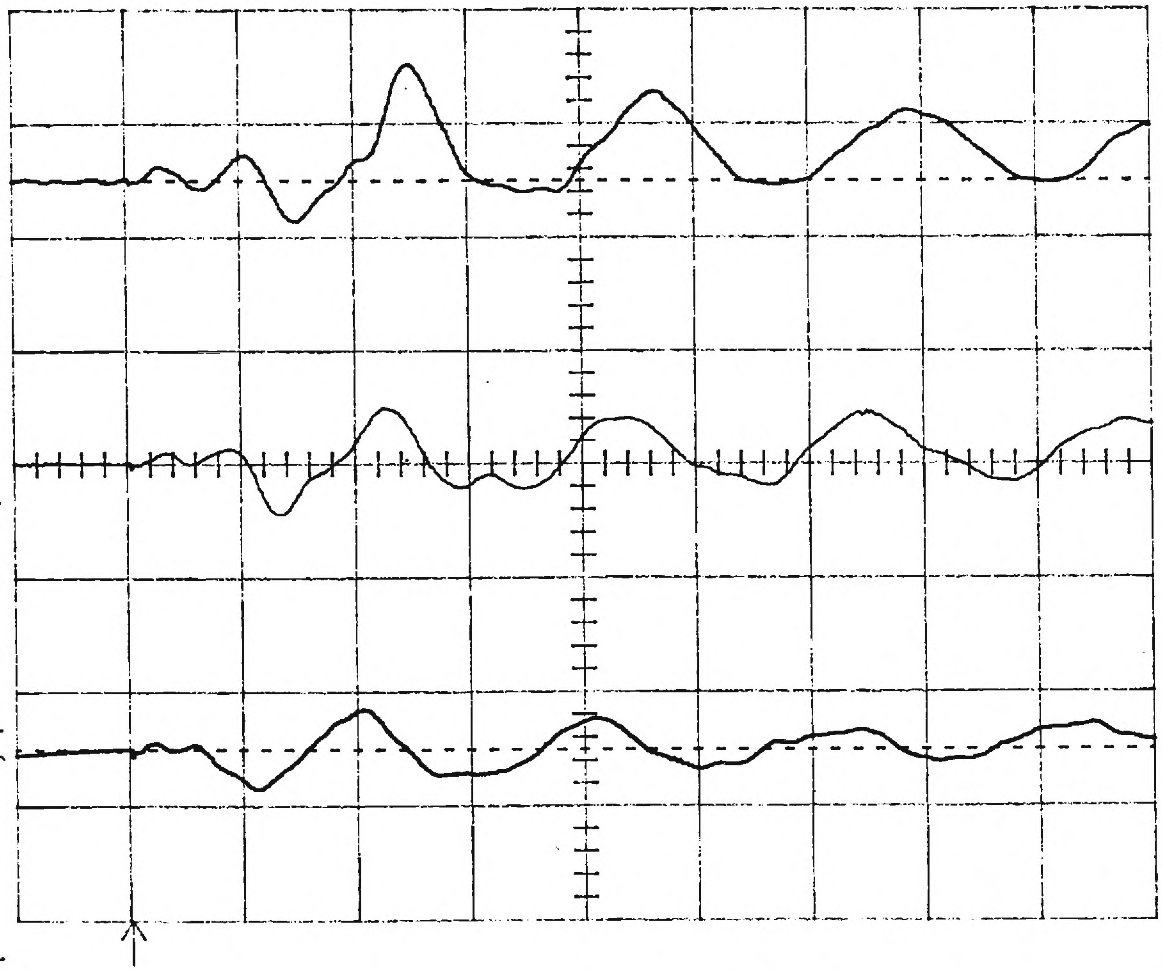

r = 4cm

Mem C
.2 ms .2 V

Mem D r = 3cm
.2 ms .2 V

<2>s 200
.2 ms .2 V

r = 2cm

anode on

EXT 1.90 V DC

BWL

CH1 50 mV x10 ~
CH2 .2 V ~
T/div .2 ms

(Cen & mid (-7.04V))
(-.03 mA current flow)

K-S 7/p
z=15cm

6-Jun-89
20:08:35

LeCroy

Main Menu

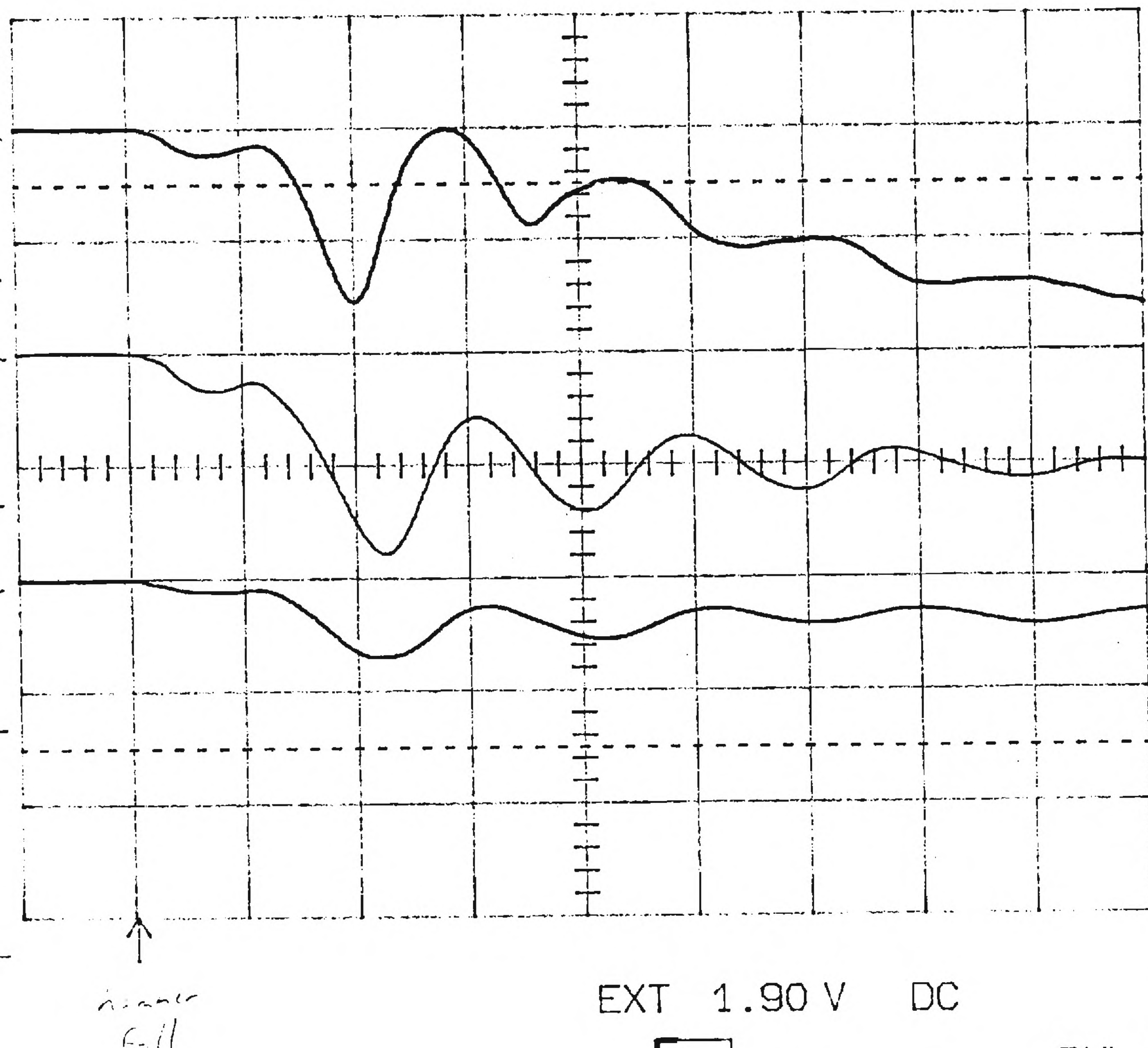

Mem C average
20 µs 2 V

Mem D average
20 µs 2 V

<1>s 200
20 µs 2 V

EXT 1.90 V DC

BWL

CH1 .2 V x10 ~
CH2 20 mV ~
T/div 20 µs

K-S v_p
15 cm

can & mid tied together & ~~floating~~
0V bias
.30 mA current

6-Jun-89
19:22:49

LeCroy

Main Menu

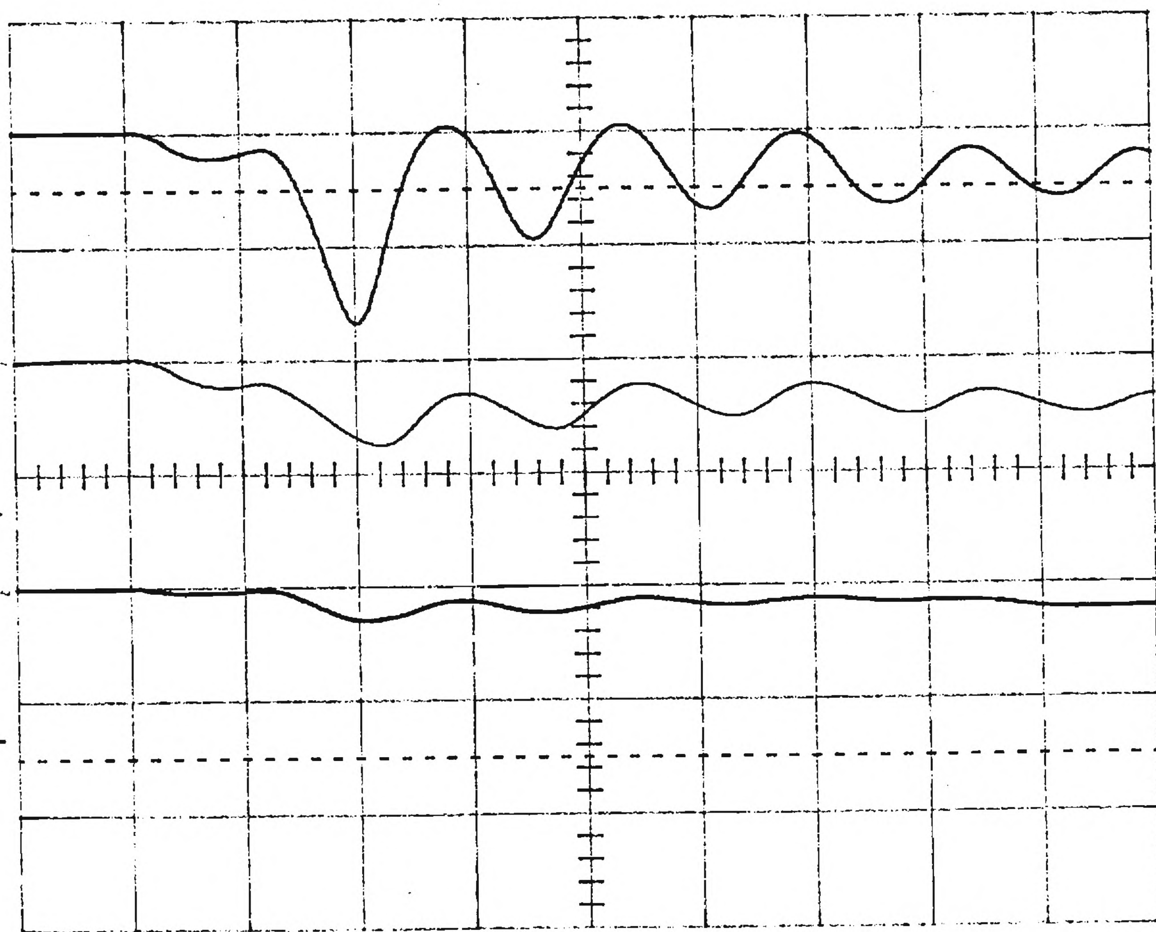

Mem C
20 µs 2 V
Mem D
20 µs 2 V
<1>s 200
20 µs 2 V

EXT 1.90 V DC

BWL

CH1 .2 V x10 ~
CH2 20 mV ~
T/div 20 µs

15

can & mid tied together & floating
.30 mA current
0 V bias

K-S V_A
z=15cm

6-Jun-89
19:09:33

LeCroy

Main Menu

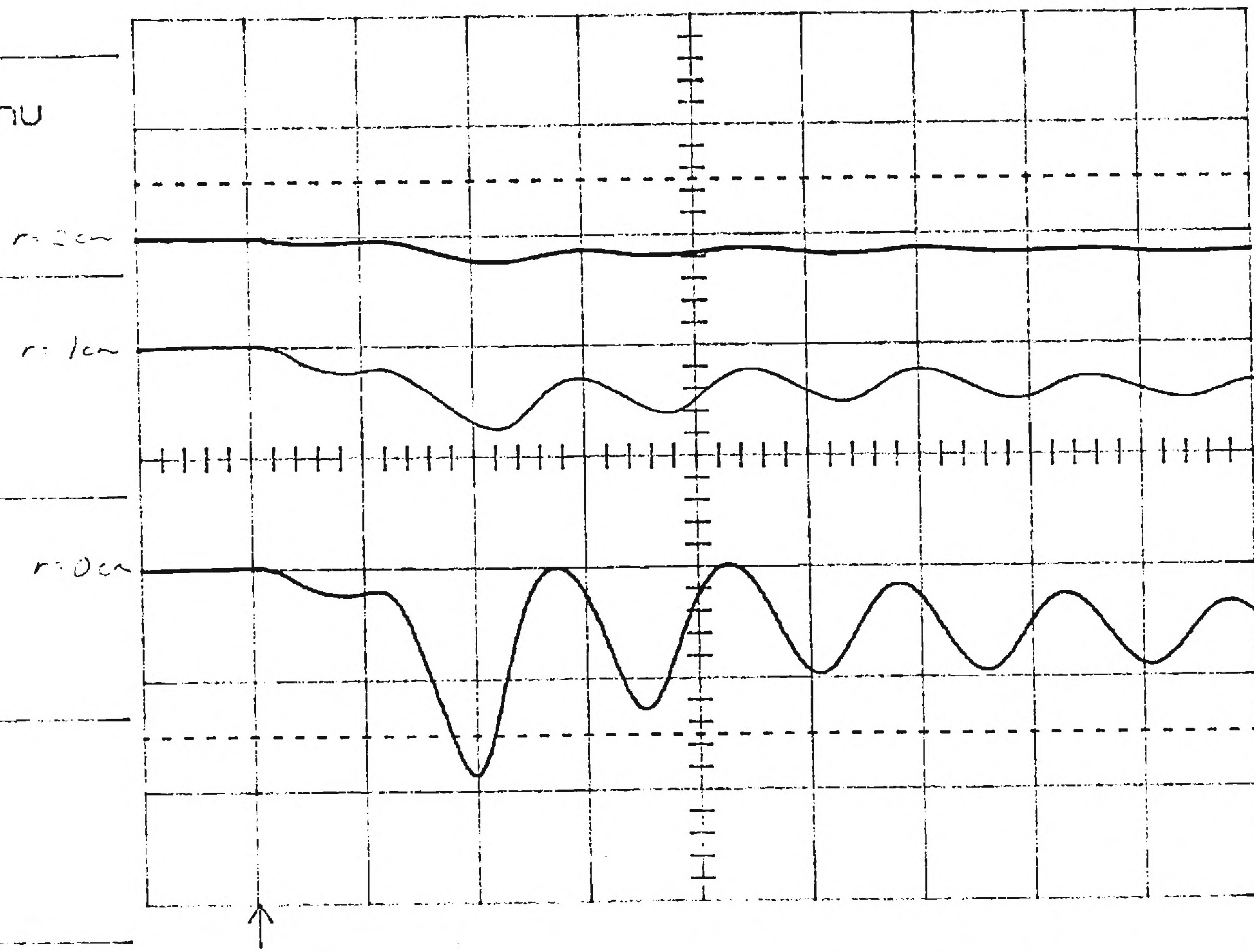

Mem C
20 µs 2 V

Mem D
20 µs 2 V

<1>s 200
20 µs 2 V

EXT 1.90 V DC

BWL

CH1 .2 V x10 ~
CH2 20 mV ~
T/div 20 µs

14

Argon 6/7/89

Ion Sat [East West]
West: z=38cm r=4.13cm
East: z=15cm r=4.13cm

cane mid tied together 0V bias
-40 mA current flow
East-Ionsat -118.8V 10kΩ D.Rox
West-Ionsat -118.8V 40kΩ Iso.A. .2V/div

7-Jun-89
17:47:54

LeCroy

Main Menu

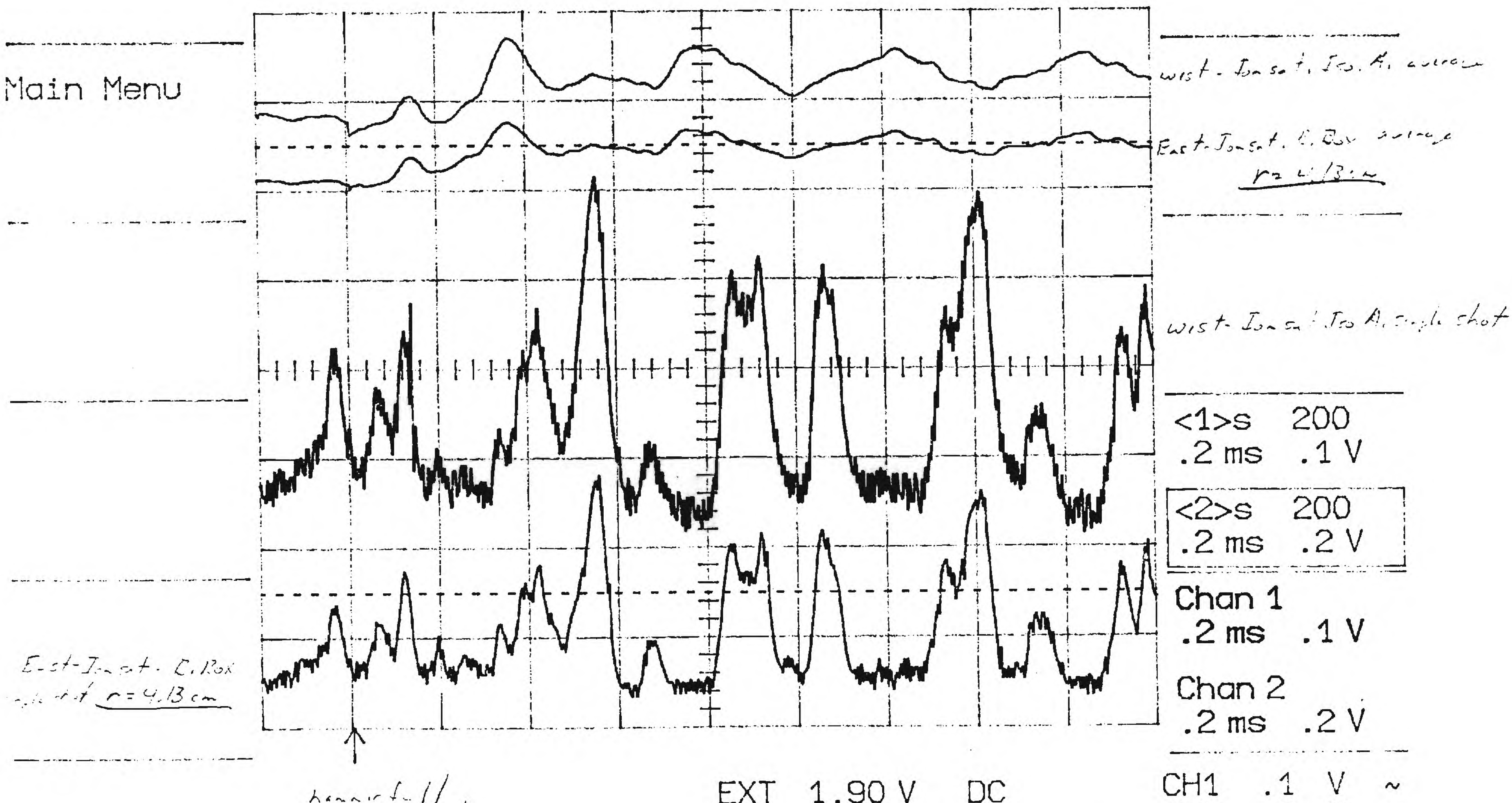

<1>s 200
.2 ms .1 V

<2>s 200
.2 ms .2 V

Chan 1
.2 ms .1 V

Chan 2
.2 ms .2 V

EXT 1.90 V DC

BWL

CH1 .1 V ~
CH2 .2 V ~

T/div .2 ms

−.36 mA current flow
East Ion Sat −119.9 V 10 kΩ R. Box
West Ion Sat −119.9 V 40 kΩ Iso. A .2 V/div

Ion Sat [East / West]
West = 39 cm r = 4.1 cm
East = 15 cm r = 4.1 cm
[West long probe ⇒ oscillating]

LeCroy

7-Jun-89
16:15:43

Main Menu

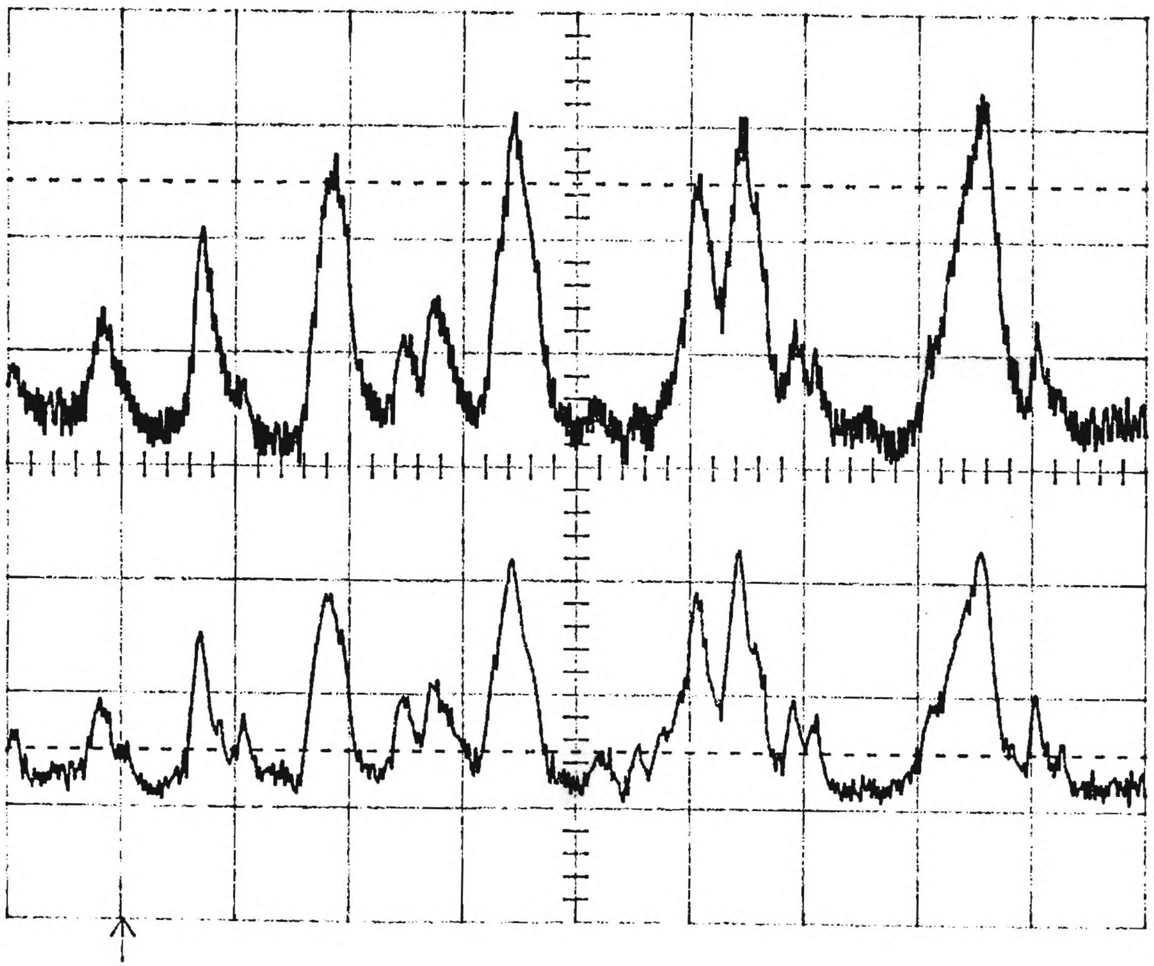

West side Ion sat
Iso. A

Chan 1
.2 ms .1 V

Chan 2
.2 ms .2 V

Rummer on

EXT 1.90 V DC

BWL

CH1 .1 V ~
CH2 .2 V ~
T/div .2 ms

21

Can & mid tied together 0V Bias
-.36 mA Current flow
East-Ioncat -119.9V 10kΩ Ri Cox
West-Ioncat -119.9V 40kΩ I∞A .2V/div

Ioncat [...]
West - 30 cm
East - 15 cm ... 4.0 cm
[West Lang probe]

LeCroy

7-Jun-89
16:20:05

Main Menu

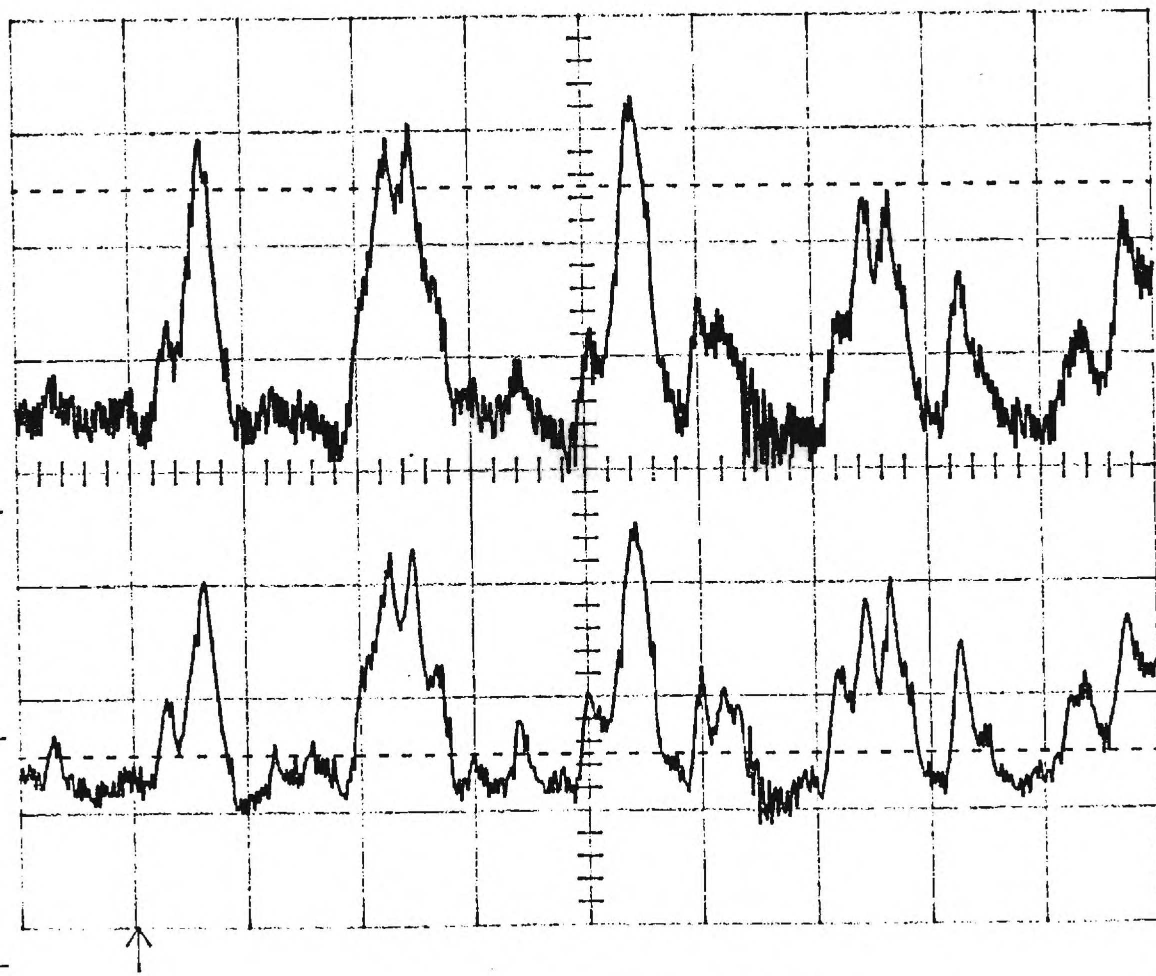

West side I∞A
Ion Cat

East side Ri Cox
Ion Cat

Chan 1
.2 ms .1 V

Chan 2
.2 ms .2 V

EXT 1.90 V DC

BWL

CH1 .1 V ~
CH2 .2 V ~
T/div .2 ms

22

-.37 mA current flow

East - Ion Sat -119.8V 10kΩ

West - Ion Sat -119.8V 4.3kΩ .2V/div

Ion Sat [East West]

West Z=37cm

East Z=15cm

LeCroy

7-Jun-89
16:29:11

Main Menu

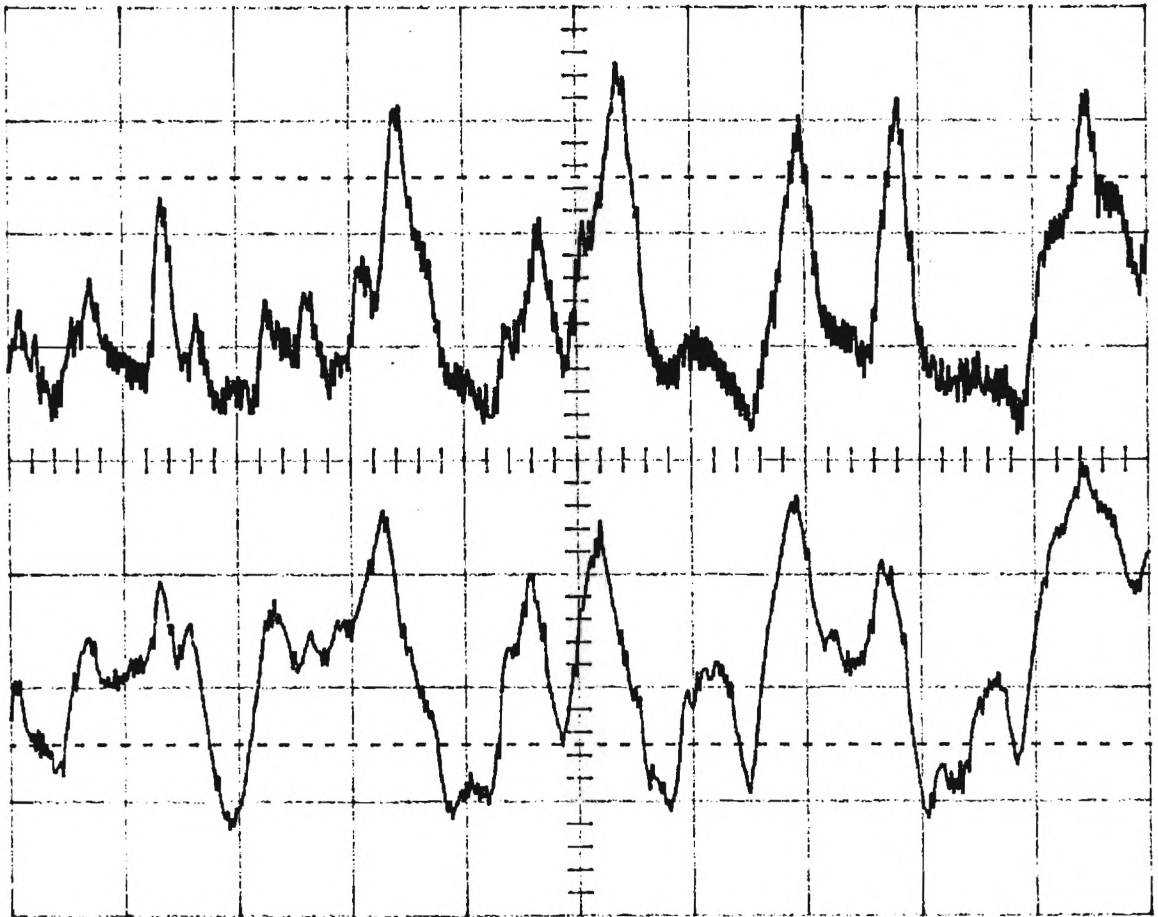

West Side Ion Sat

East side Ion Sat
B. Box

Chan 1
.2 ms .1 V

Chan 2
.2 ms .2 V

hammer fall

EXT 1.90 V DC

BWL

CH1 .1 V ~
CH2 .2 V ~
T/div .2 ms

Can & emit tied together 0 V Bias
-.37 mA current flow
East Ion Sat -118.8V 10kΩ R, Roy
West Ion Sat -118.8V 40kΩ I-sat, .2 V/div

Ion Sat [East West
West: z=39cm r=4.15cm
East: z=15cm r=2cm

LeCroy

7-Jun-89
16:32:55

Main Menu

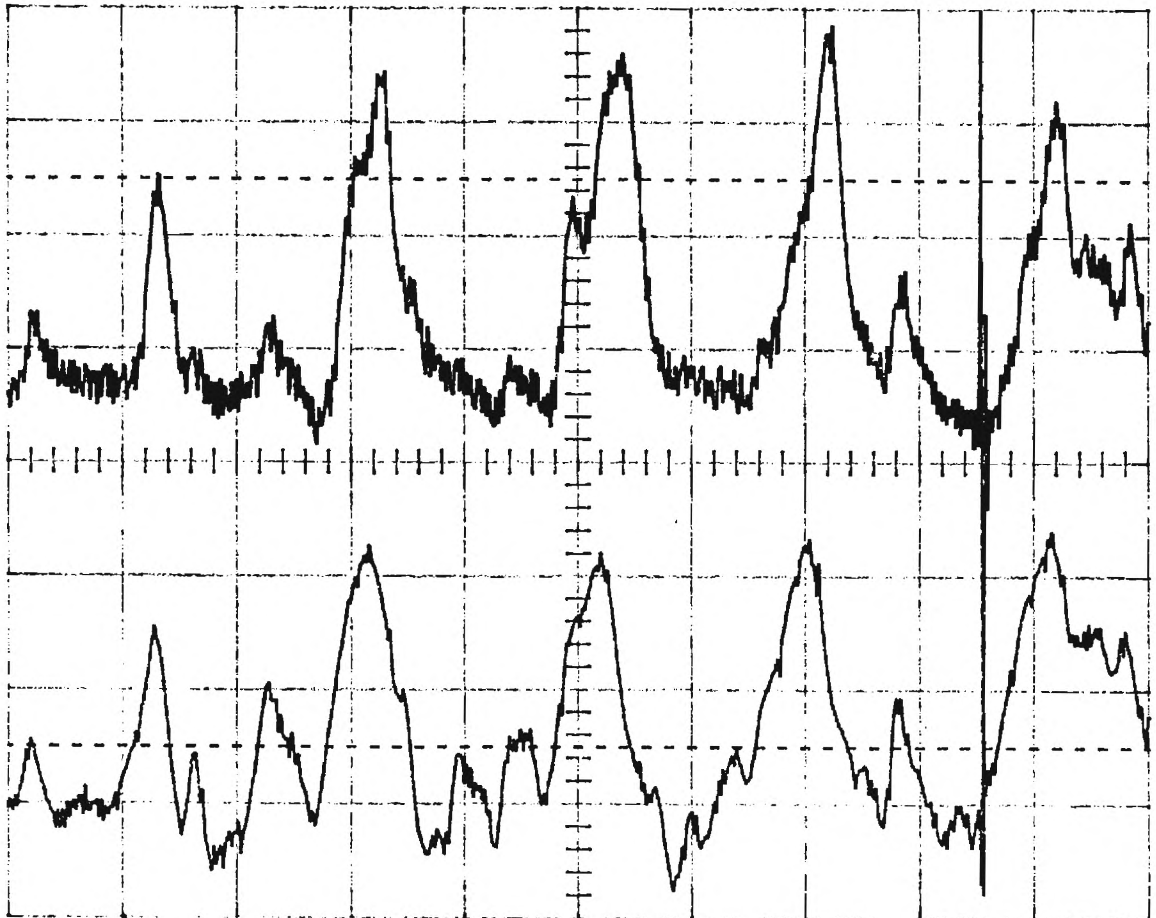

Mem C .2 ms .1 V
West side Ion Sat I-sat,

Mem D .2 ms .2 V

East side Ion Sat
R, Roy

trigger

EXT 1.90 V DC

BWL

CH1 .1 V ~
CH2 .2 V ~
T/div .2 ms

24

Can & mad tied together 0V Bias
−.37 mA current flow
East - Ion Sat −118.8 V 10 kΩ R. Rox
West - Ion Sat −118.8 V 40 kΩ Iso Amp. .2 V/DIV

Ion Sat [East / West]
West z = 37 cm r = 4.75 cm
East z = 15 cm r = 3 cm → 2 cm

LeCroy

7-Jun-89
16:39:53

Main Menu

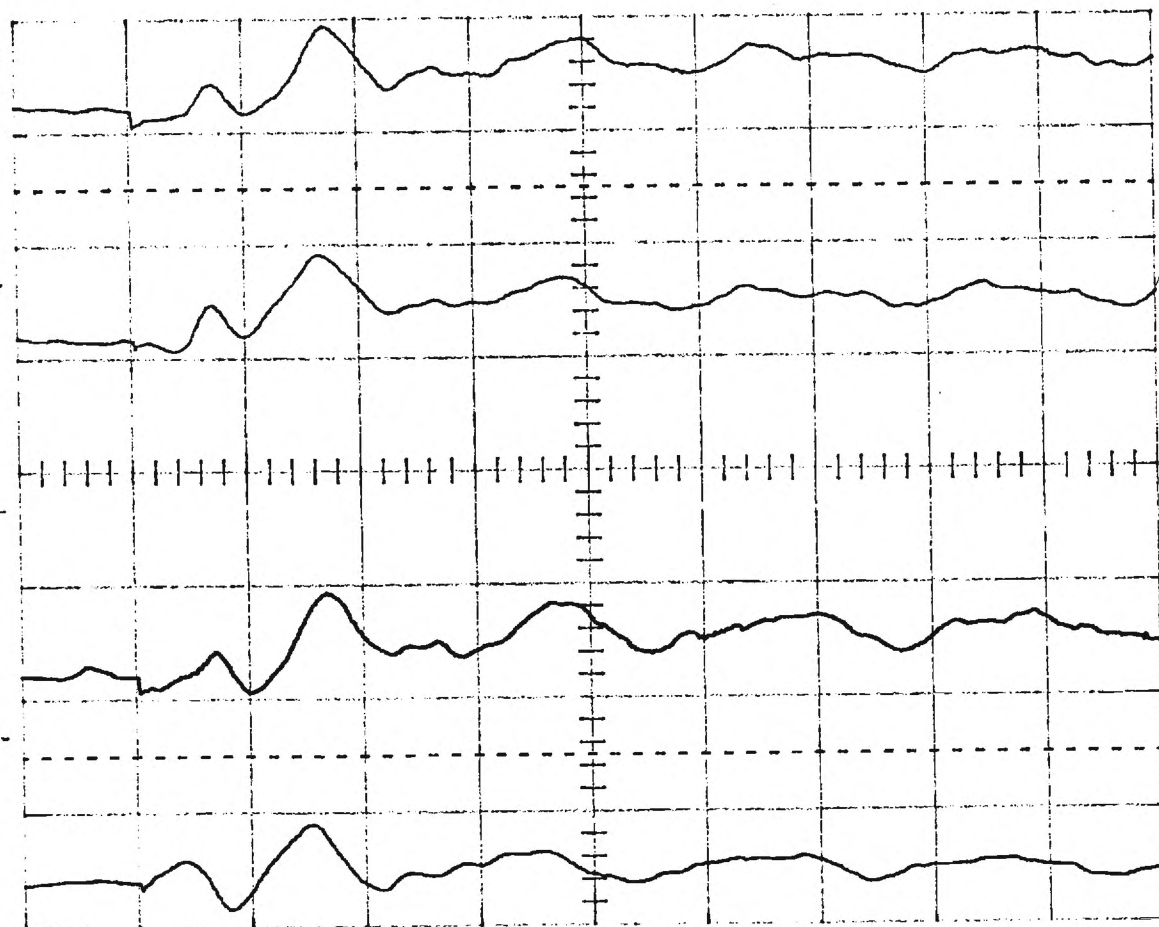

West side Ion Sat Iso Amp

East side Ion Sat R. Rox r = 3 cm

Mem C
.2 ms .1 V

Mem D
.2 ms .2 V

<1>s 200
.2 ms .1 V

West Ion Sat Iso Amp

<2>s 200
.2 ms .2 V

East Ion Sat R. Rox r = 2 cm

hammer fall

EXT 1.90 V DC

BWL

CH1 .1 V ~
CH2 .2 V ~
T/div .2 ms

Cone mid tied together 0 V Bias
−.40 mA current flow
East-Ion Sat −118.8 V 10 kΩ B. Box
West-Ion Sat −118.7 V 40 kΩ Tex.A. .2 V/div

Ion Sat [East / West
West: z ≈ 39 cm r ≈ 4.13 cm
East: z ≈ 15 cm r ≈ 2 cm

LeCroy

7-Jun-89
16:48:52

Main Menu

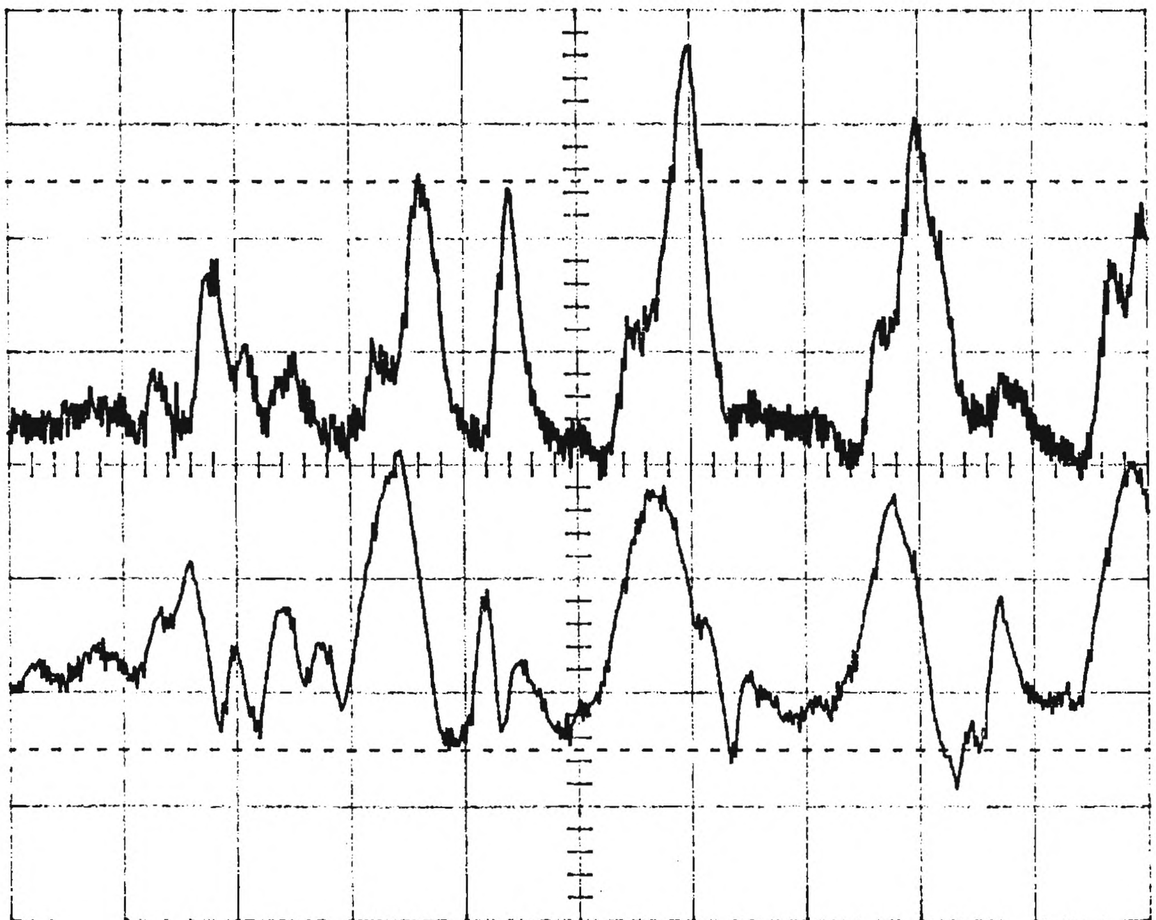

West side Ion Sat
Tex. A.

East side Ion Sat
B. Box r = 1 cm

Chan 1
.2 ms .1 V

Chan 2
.2 ms .2 V

hammer fall

EXT 1.90 V DC

BWL

CH1 .1 V ~
CH2 .2 V ~
T/div .2 ms

26

Can emit tied together 0V line
~10 mA current flow
East-Insert -118.8V 10kΩ
West-Insert -118.8V 40kΩ

7-Jun-89
16:55:10

LeCroy

Main Menu

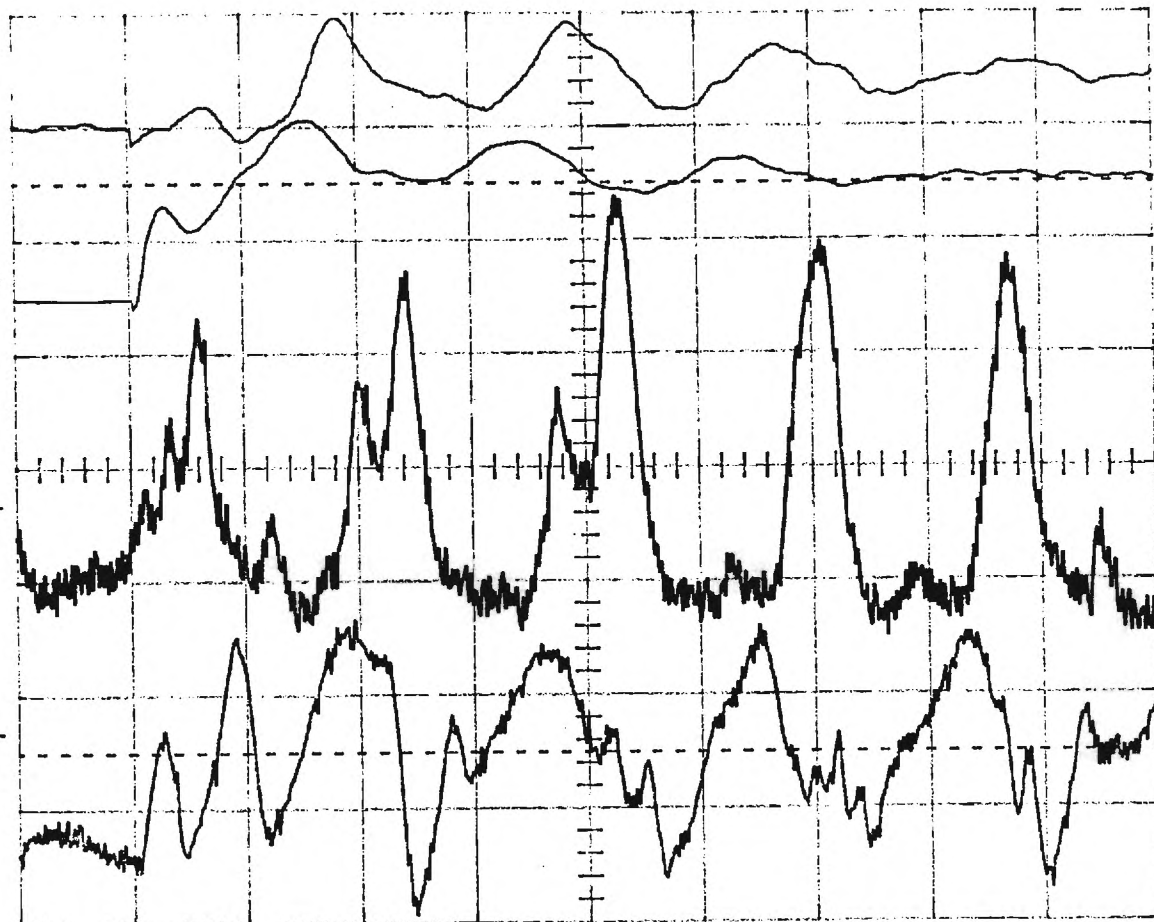

hammer fall

Mem C
.2 ms .1 V

Mem D
.2 ms .2 V

<1>s 200
.2 ms .1 V

<2>s 200
.2 ms .2 V

EXT 1.90 V DC

BWL

CH1 .1 V ~
CH2 .2 V ~
T/div .2 ms

27

Cant wid tied together OV Bias
-.39 mA current flow
East - Ion Sat -118.8 V 10kΩ B.Box
West - Ion Sat -118.8V 40kΩ Iso.A, .2V/div

Ion Sat West/East 6/7/89
West: z=37cm r=4.13cm
East: z=15cm r=0cm

LeCroy

7-Jun-89
17:02:28

Main Menu

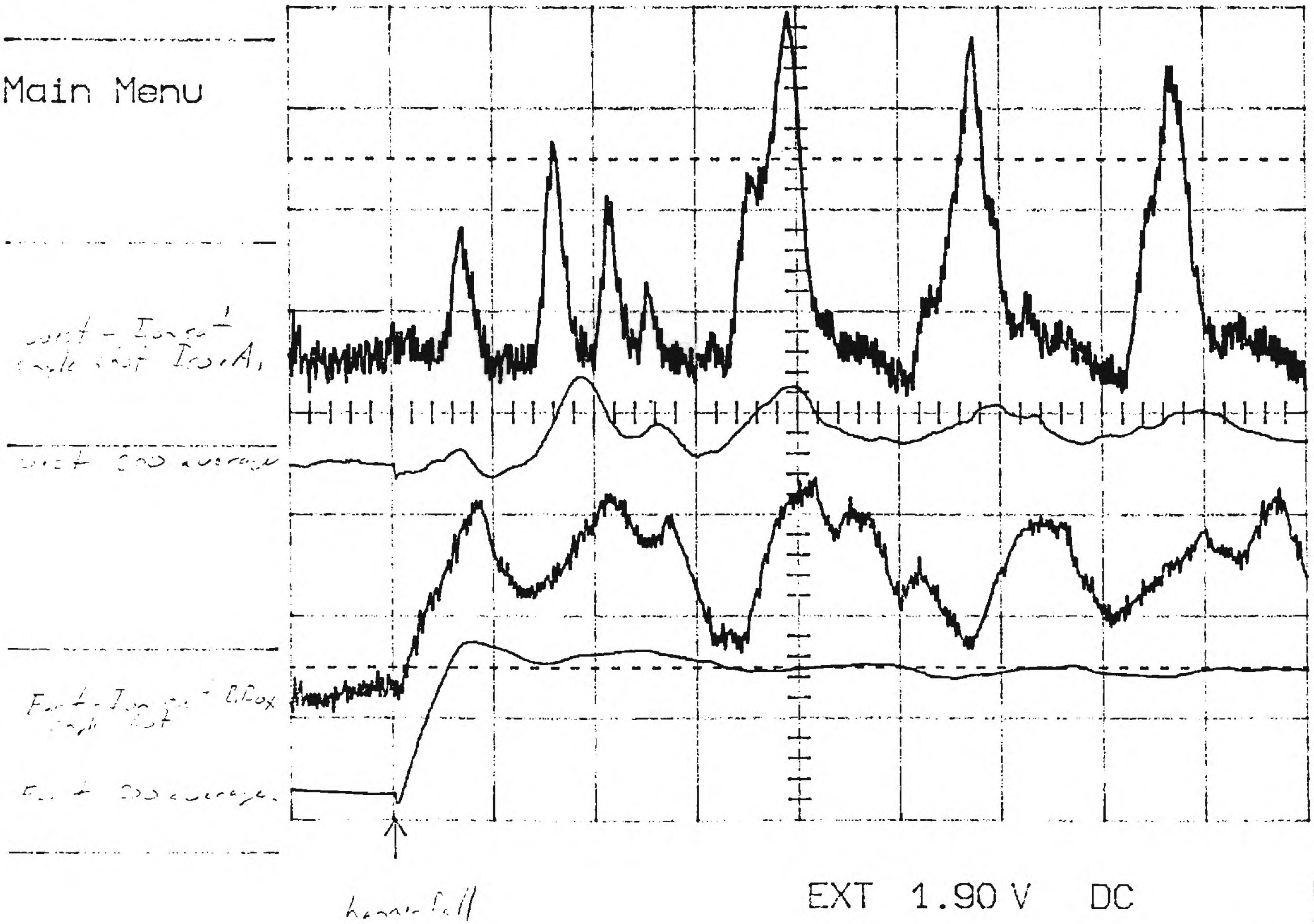

Mem C
.2 ms .1 V

Mem D
.2 ms .2 V

Chan 1
.2 ms .1 V

Chan 2
.2 ms .2 V

EXT 1.90 V DC

BWL

CH1 .1 V ~
CH2 .2 V ~
T/div .2 ms

(28)

51

E

Main
Menu KS

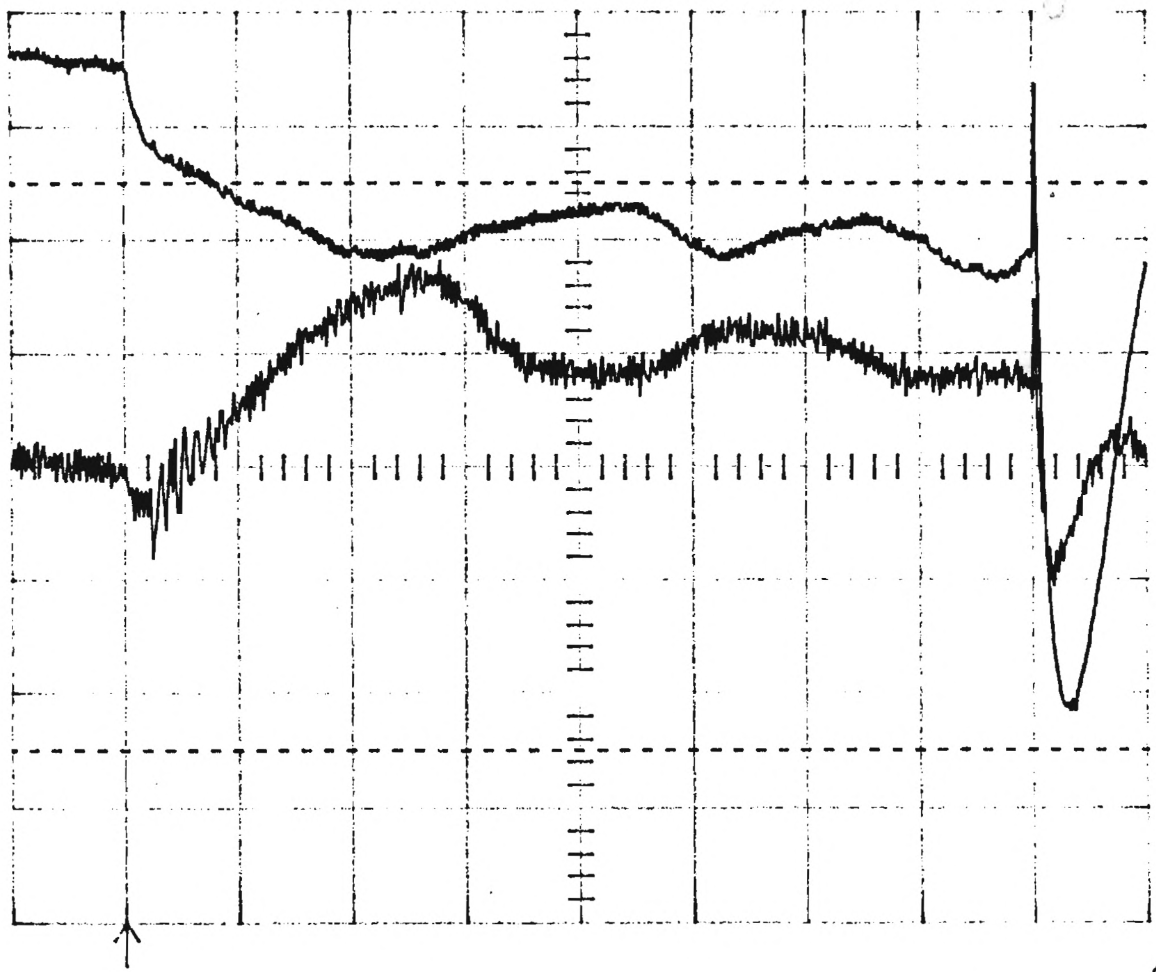

W

Ion Sat

Channel 1 E. K
.1 ms 1 V

Channel 2
.1 ms .2 V W

Ch 1 1 V =
T/div .1 ms Ch 2 .2 V =
Trig .46 V + EXT <

E + 2° 1257

W − 3° 1280

Outer + Anvil current Cu plate → Gnd
middle and Can unknown

I.S.: R = 50kΩ

Amp. @ .1V/div

52

East KS

Main
Menu

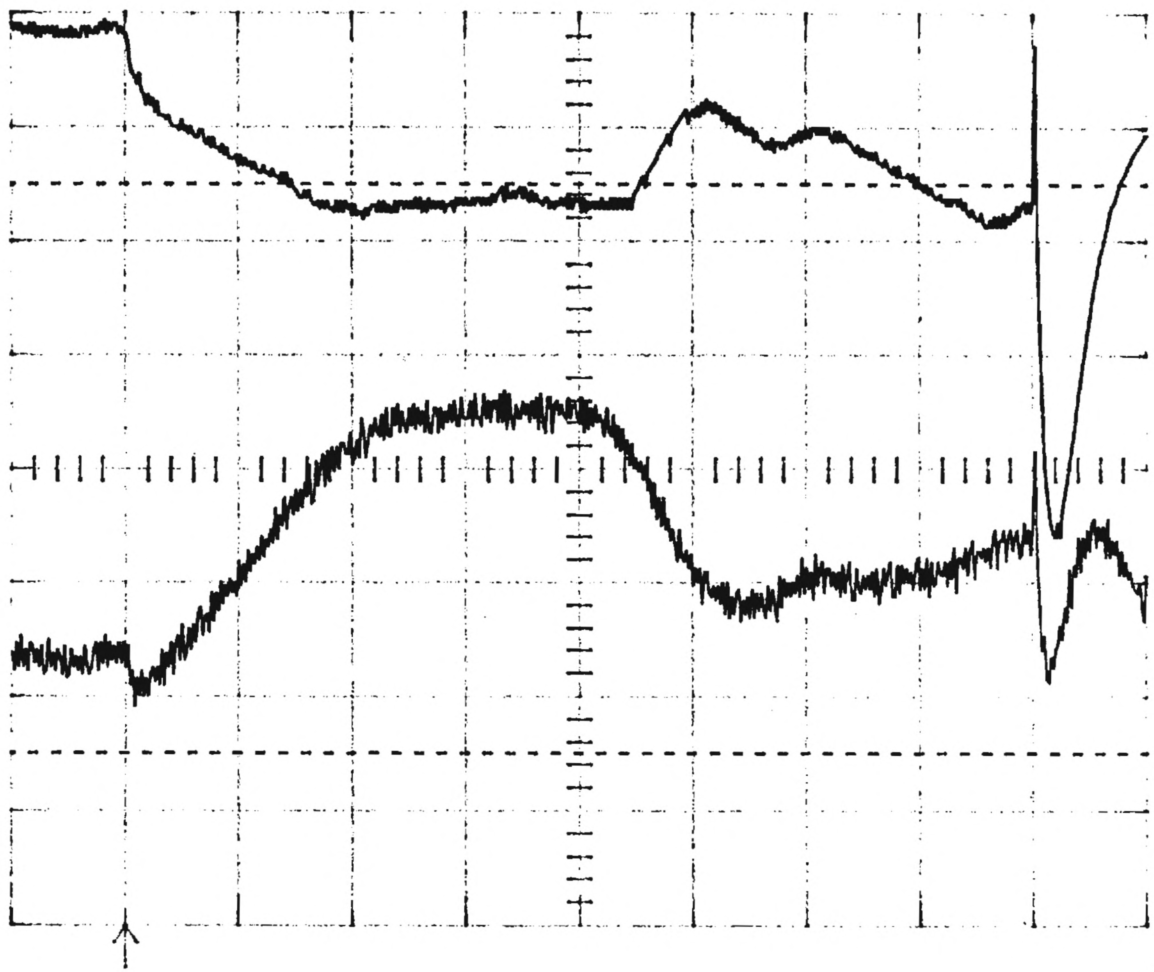

W
ion sat

Channel 1
.1 ms 1 V

Channel 2
.1 ms .2 V

Ch 1 1 V =
T/div .1 ms Ch 2 .2 V =
Trig .46 V + EXT <

Voltage → 1.136 V on can & middle screen

Outer anvil screen + plate = Gnd

SRS #1

E +2° 1257

W -3° 1280

East K.S. offset bias = 0V
West J.S. bias = 0V
K.S. Heater = .53V

J.S.: R = 50kΩ
Ion. Amp. @ .1V/div

(53)

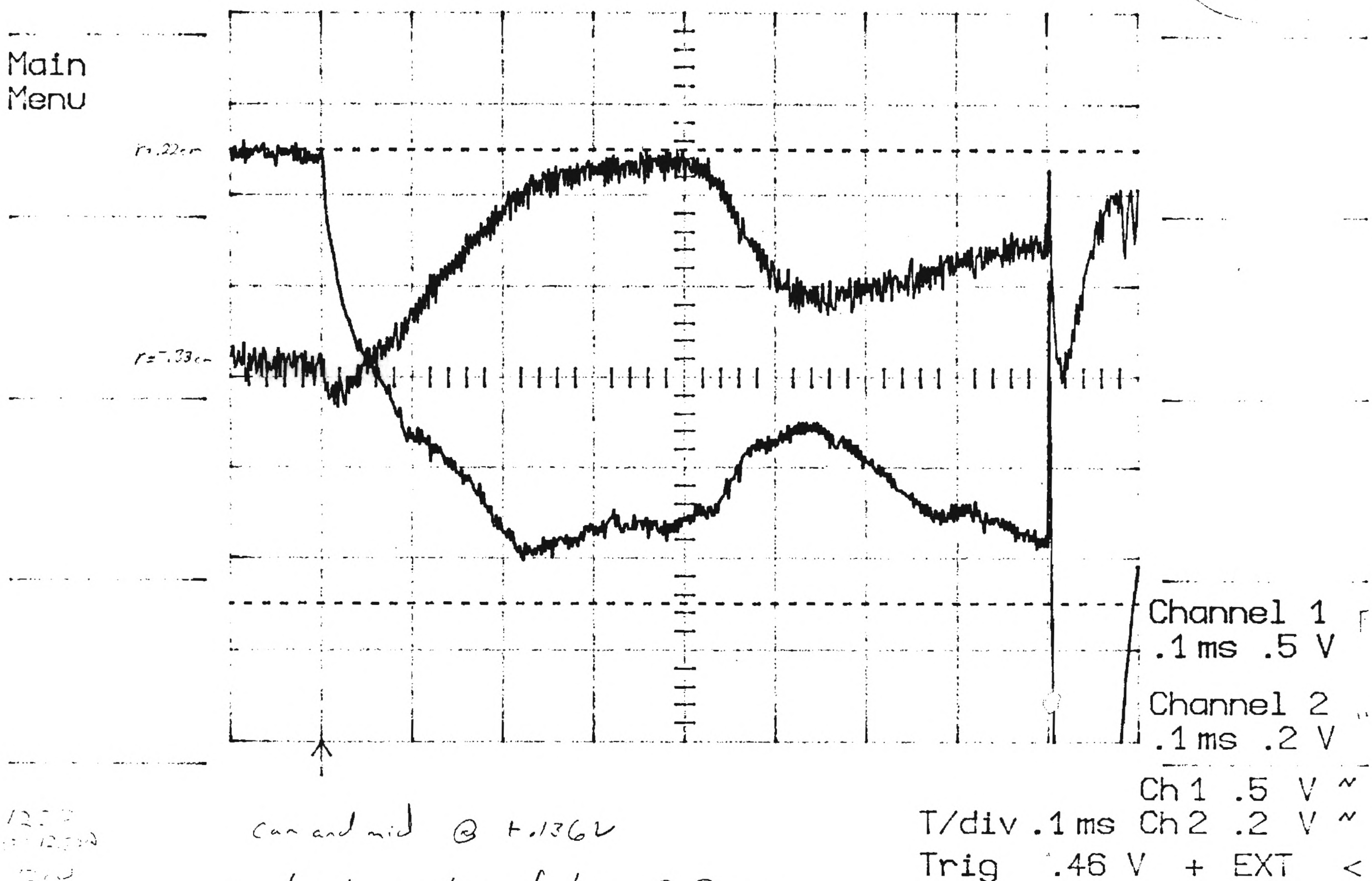

Can and mid @ +.136V

center to center of lips 2.5 mm
Outer Anvil current Cu plate = Gnd
chan # 1

I.S.: R = 50kΩ
Ins. Amp. @ .1 V/div

54

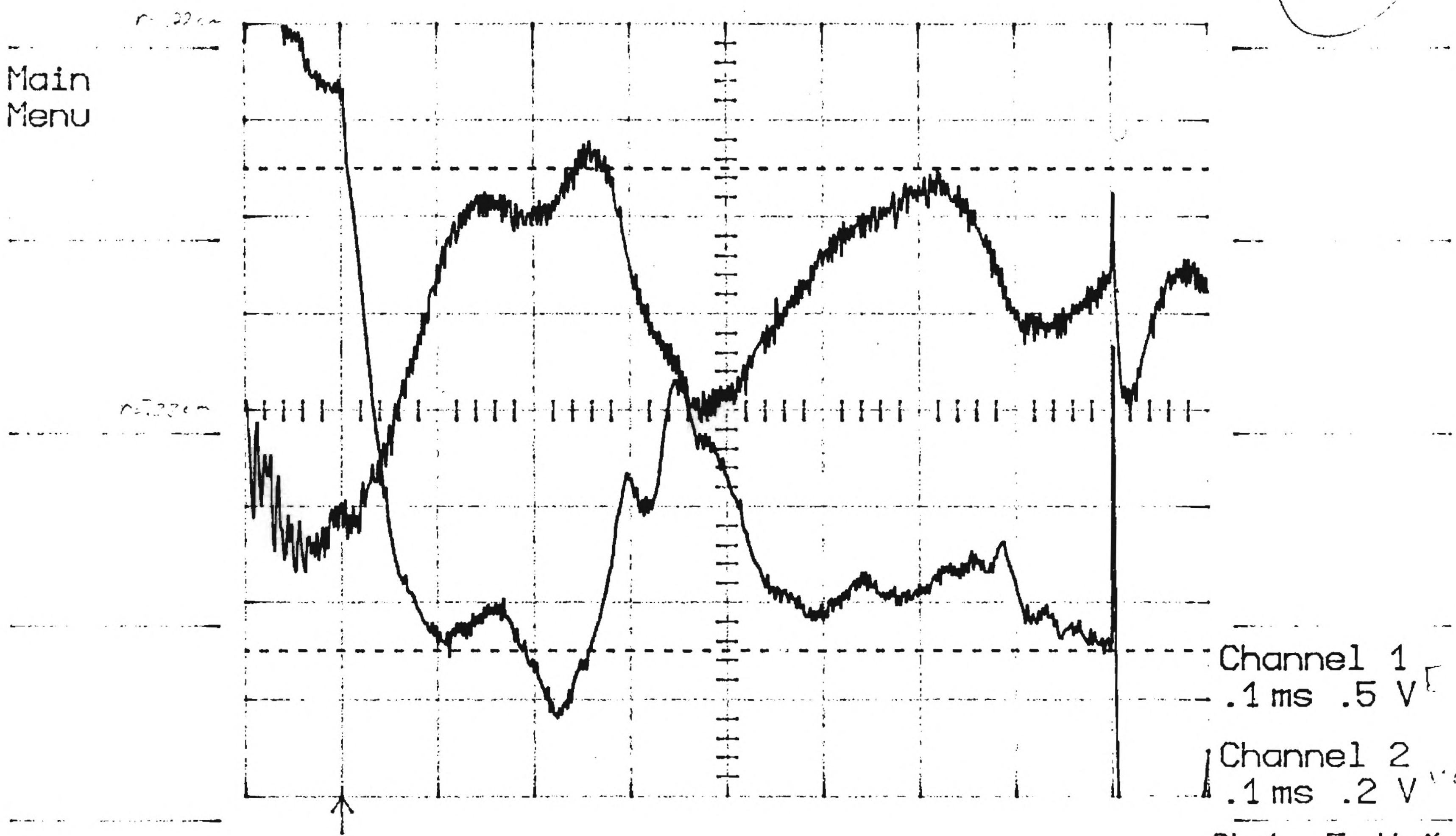

Outer + Anvil Screen + Cap plate = Gnd
Can + mid = unknown

SRS # 1

I +2 1257

W -3 1326

[illegible]
[illegible]
[illegible]

I.S.: R = 50 kΩ
Ion. Amp 0.1 V/Div

55

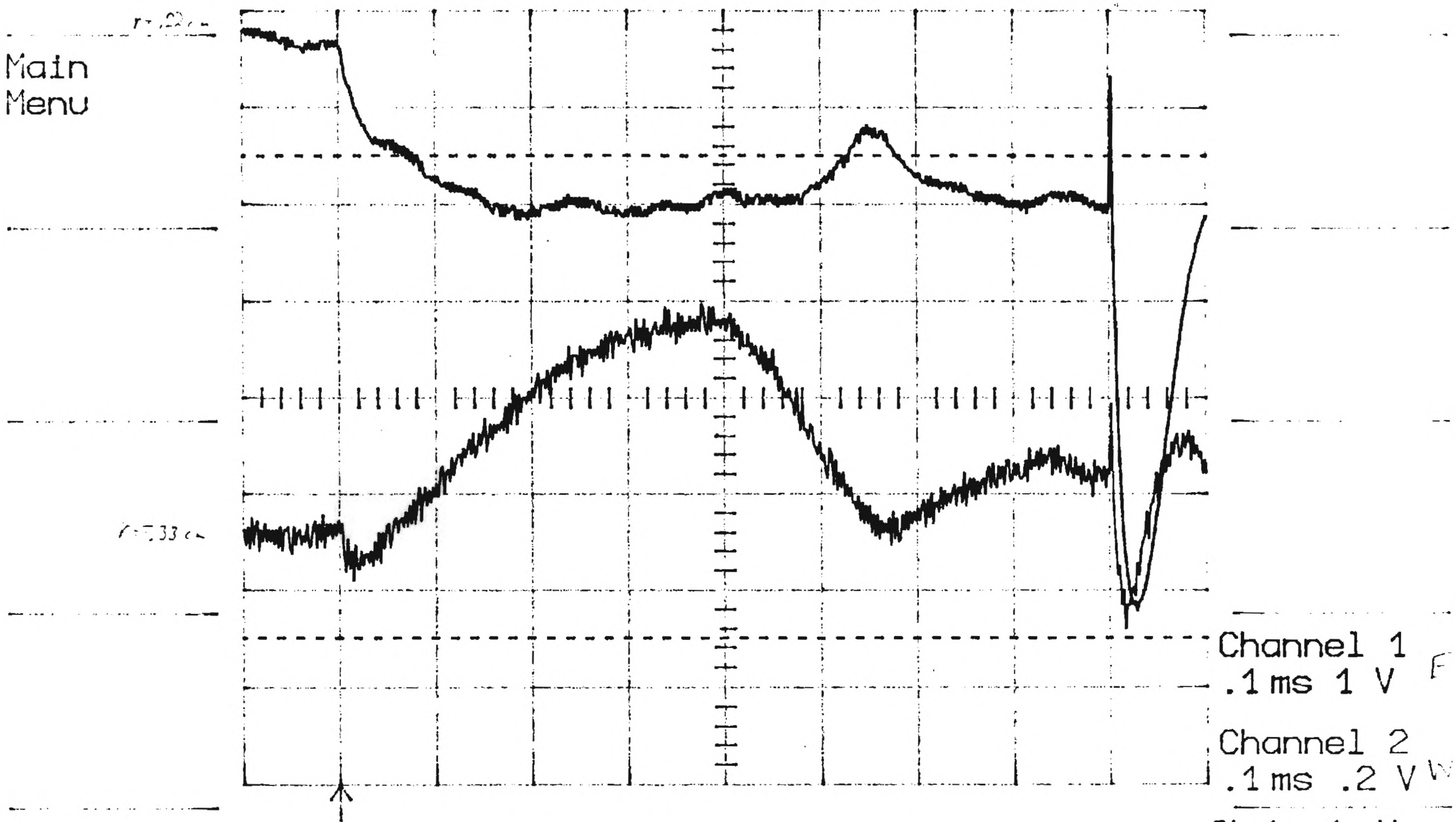

Ch 1 1 V =
T/div .1 ms Ch 2 .2 V =
Trig .46 V + EXT <

F +0° 1034
W −3° 1280

Outer + Anvil screen + Cu plate = Gnd
middle and Can unknown

SRS #1

Run # 5

East: K.S. ... = ...v
West: I.S. ...
K.S. ... = ...v

I.S.: R = 50 kΩ
Jun Amp @ .1v/div

56

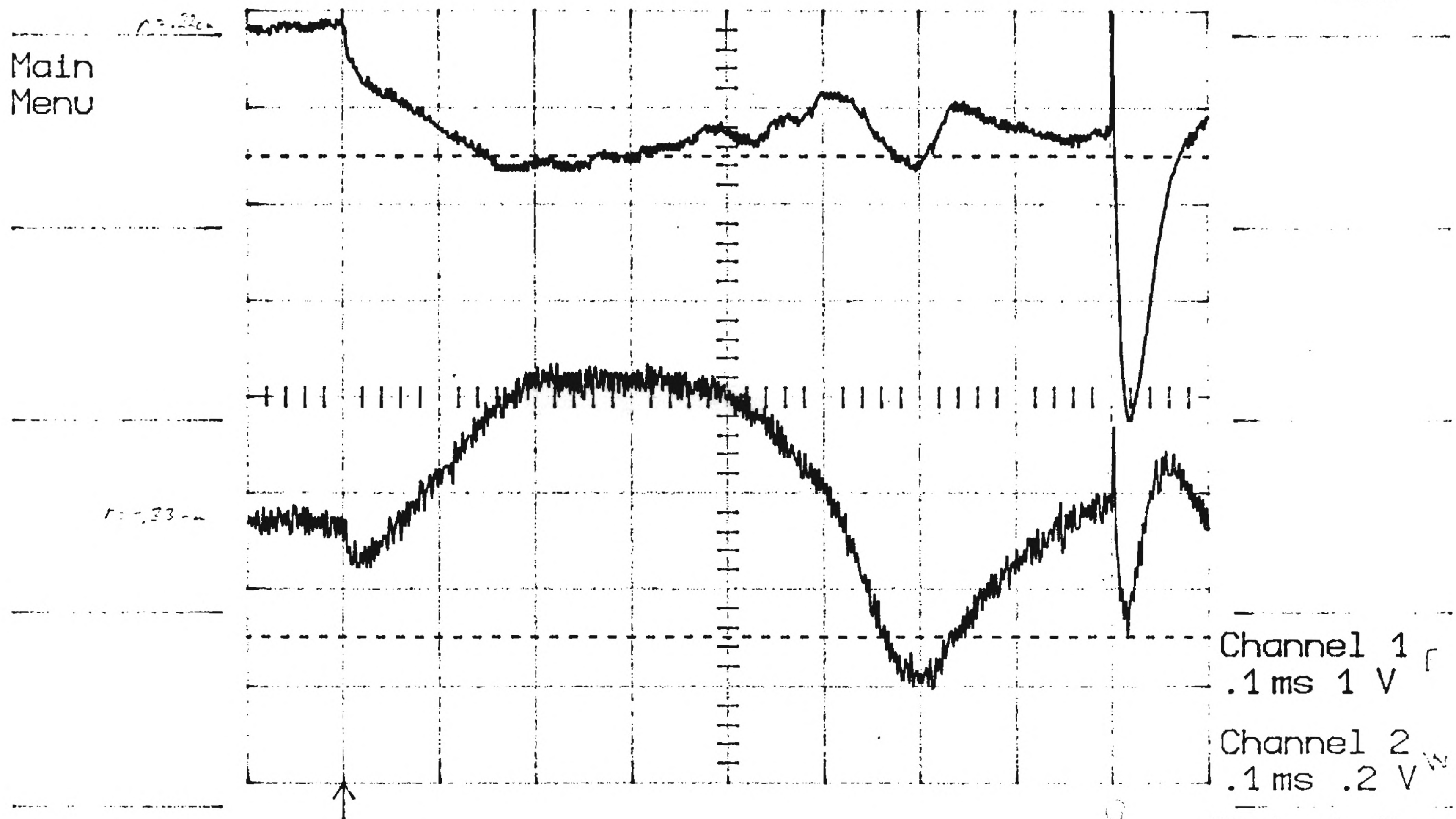

E +2° ·1257

W -3° 1280

Outer + Anvil screen + Cu plate = Gnd
middle and can unknown

CRS # 1

Ext: V.C. = 0V
wst: I.S. V
K.C. Heater = .55V

Individual Trace I.S.: R=10kΩ
Ion Amp. 0.1V/div

No averaging

57

Main
Menu

E

r=.22cm

W

r=-.33cm

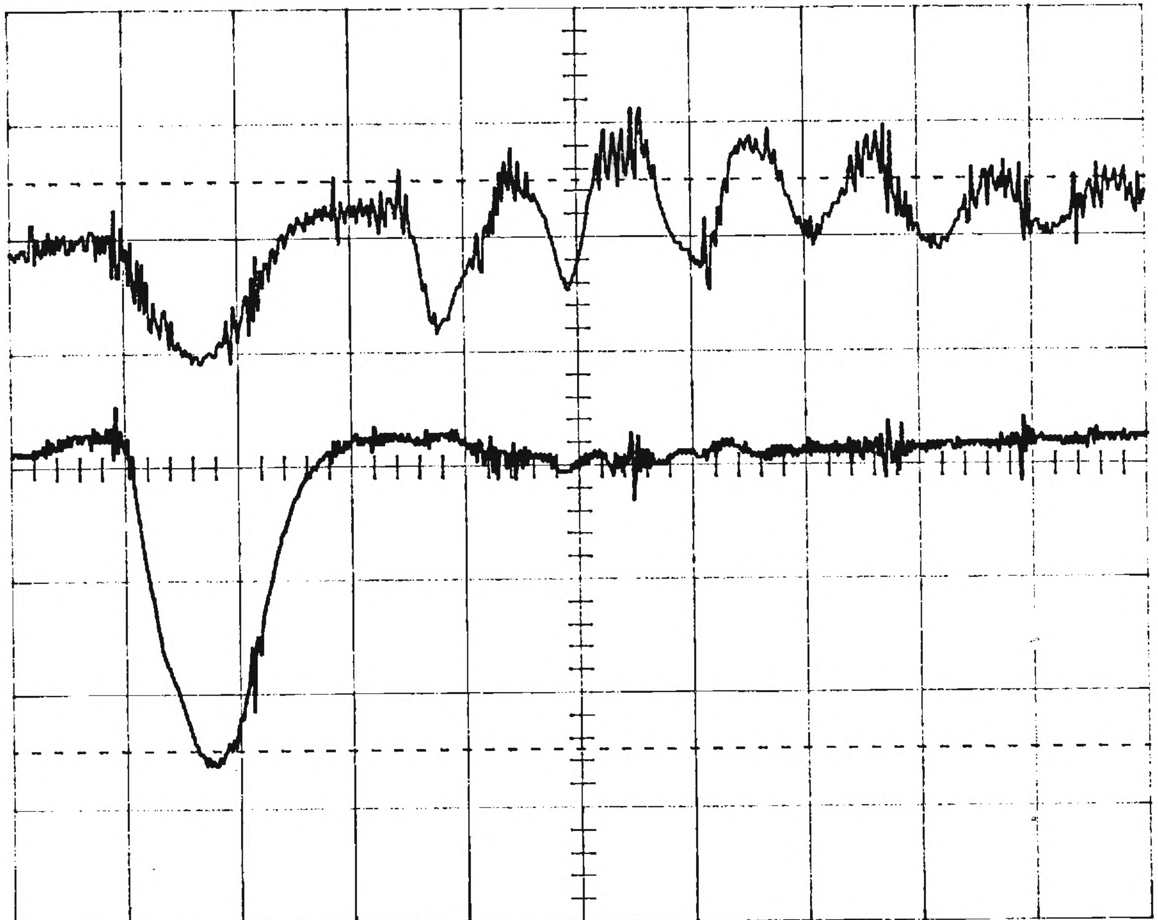

Plasma
Potential

Ion
Saturation

Channel 1
10 µs .2 V

Channel 2
10 µs .1 V

Outer = Gnd
Anvil Screen + Cup plate = Gnd
Can + Green @ 5V

Ch 1 .2 V ~
T/div 10 µs Ch 2 .1 V ~
BWL Trig .48 V + EXT

CRS#9

East: K.S. offset bias = 0v
Heater = .52V
West: I.S. bias = -80v
R = 50 kΩ
Iso. Amp. @ .1v/div

5/11/99

101

Main
Menu

E (KS)

r = 4.00 cm

W

r = -2.63 cm

Ion Sat

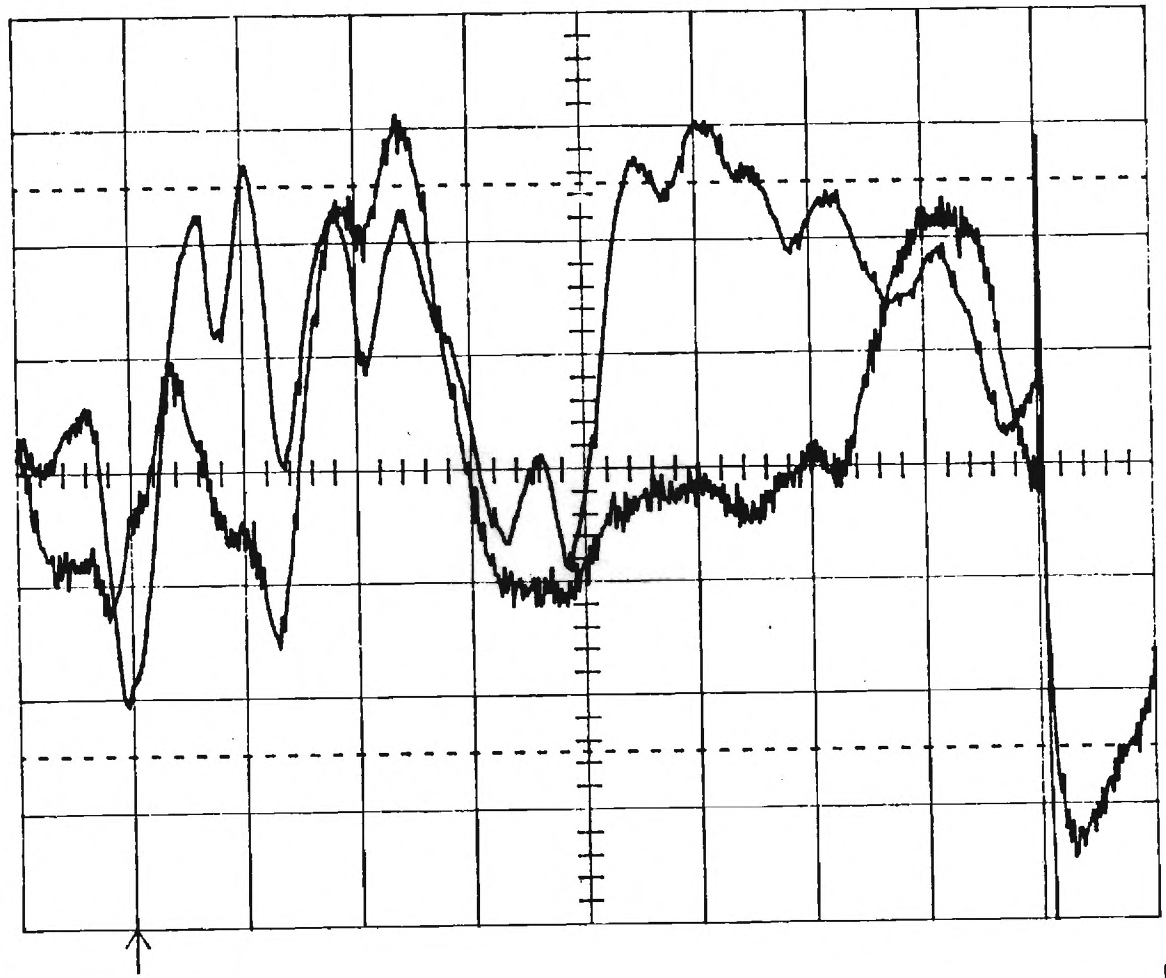

Channel 1 East; 0007; +36.7 =
.1 ms .5 V

Channel 2 West; -23.9° 03000
.1 ms .2 V

Ch 1 .5 V ~
T/div .1 ms Ch 2 .2 V ~
Trig .49 V + EXT <

E: 36.7° 0071
r = 4.00 cm
W: -23.9° 3000

Outer guide can = Gnd
Anvil Screen & Cu Plate = 0v
SRS #8
R.A 190 ms

Marconi @ 747.5 MHz @ -11 dBm

East: K.S. offset bias = 0v
Heater = .52v
West: I.S. bias = -80v
R = 50 kΩ
Iso. Amp. @ .1V/div

(102)

Main
Menu

W
Ion Sat

r = 4.00 cm

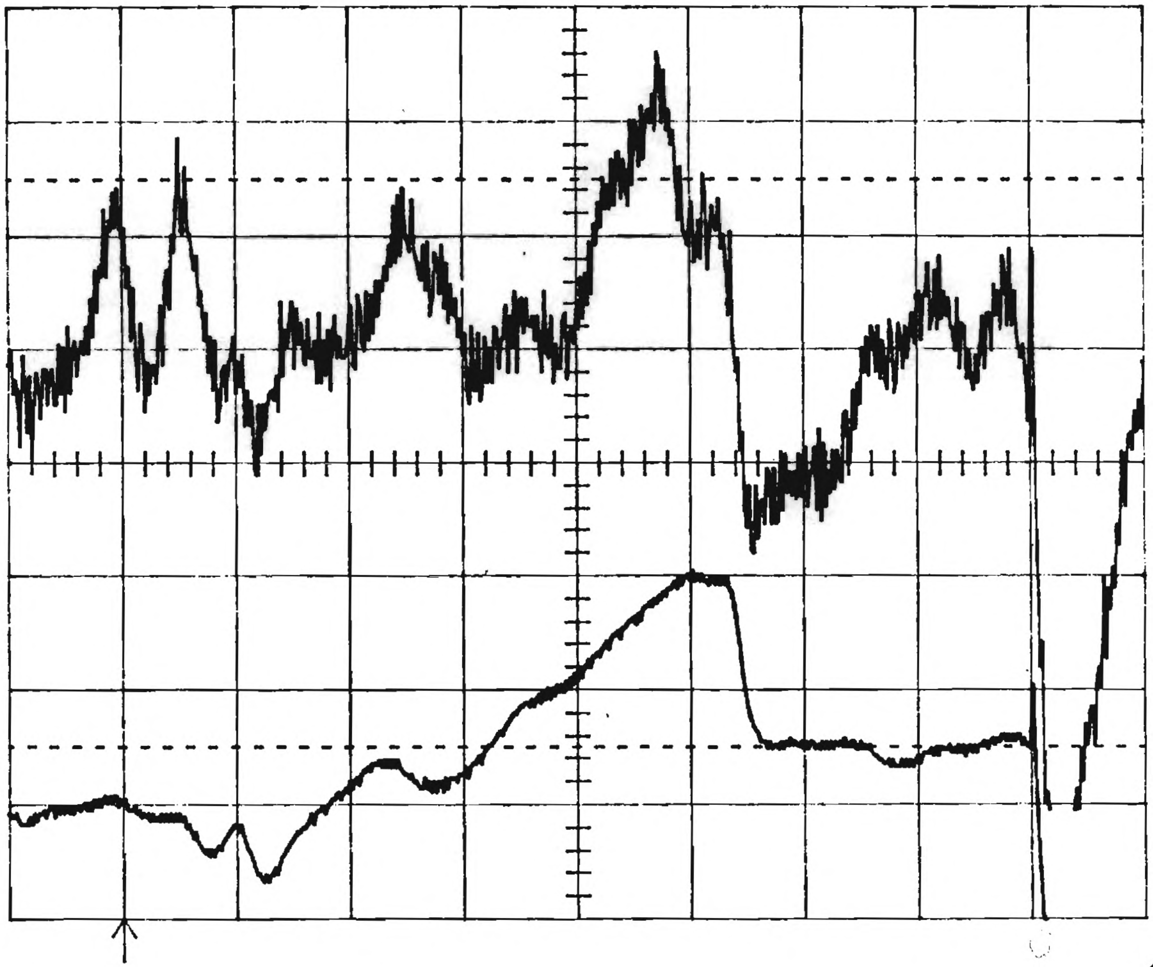

E
KS

r = 4.00 cm

Channel 1 East 0.000 -36.7
.1 ms 2 V
Channel 2 West 0.000 +36.7
.1 ms .1 V
Ch 1 2 V ~
T/div .1 ms Ch 2 .1 V ~
Trig .49 V + EXT <

E: -36.7° 1000
r = 4.00 cm
W: +36.7° 4000

Outer anode can = Gnd
Anvil Screen & Cu Plate = 0v
SRS #8
B = A 170 ms

Marconi: 747.5 MHz @ -11 dbm

East: K.S. offset bias = 0V
Heater .52V
West: I.S. bias = -80V
R = 50 kΩ
Iso. Amp. @ .1V/div

as 40; 25

103

Main
Menu

W
Io. Sat
r = 4.00cm

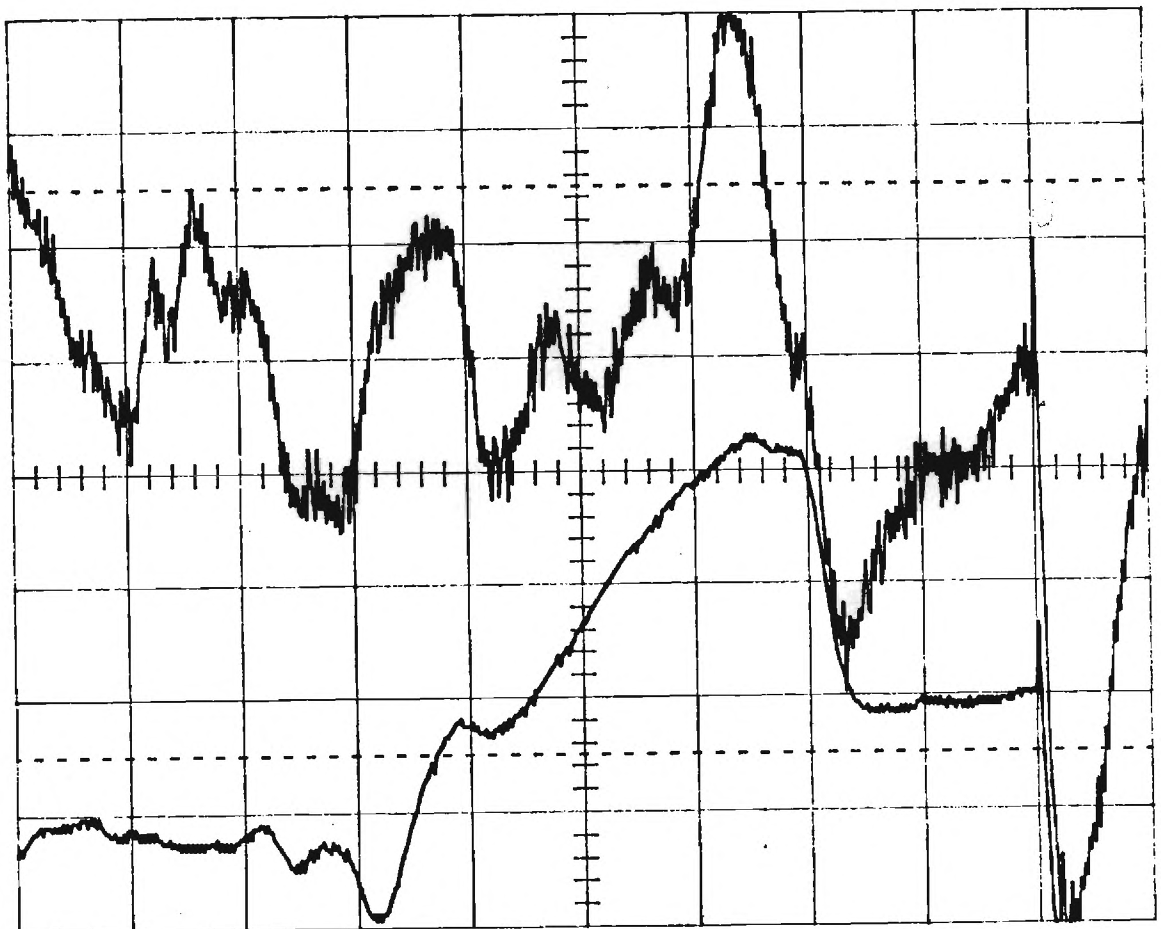

E
KS
r = -4.00cm

Channel 1 Fast
.1 ms 2 V K.S.

Channel 2 West
.1 ms .1 V I.S.

Ch 1 2 V ~
T/div .1 ms Ch 2 .1 V ~
Trig .49 V + EXT <

E: -36.7° 1000
r = -4.00cm
W: +36.7° 1000

Outer side can = Gnd
Anvil screen Cu Plate = 0V
SRS #8
B = A + 90ms

Marconi: 747.5 MHz @ -11 dBm

East: K.S. offset bias = 0v
Heater = .52V

West: I.S. bias = -80v
R = 50kΩ
Iso. Amp. @ .1V/div

40; 29

as 25

except
Mid Screen → -76

5/11/8?

104

Main
Menu

E KS r=4.00cm

W Ion Sat r=4.00cm

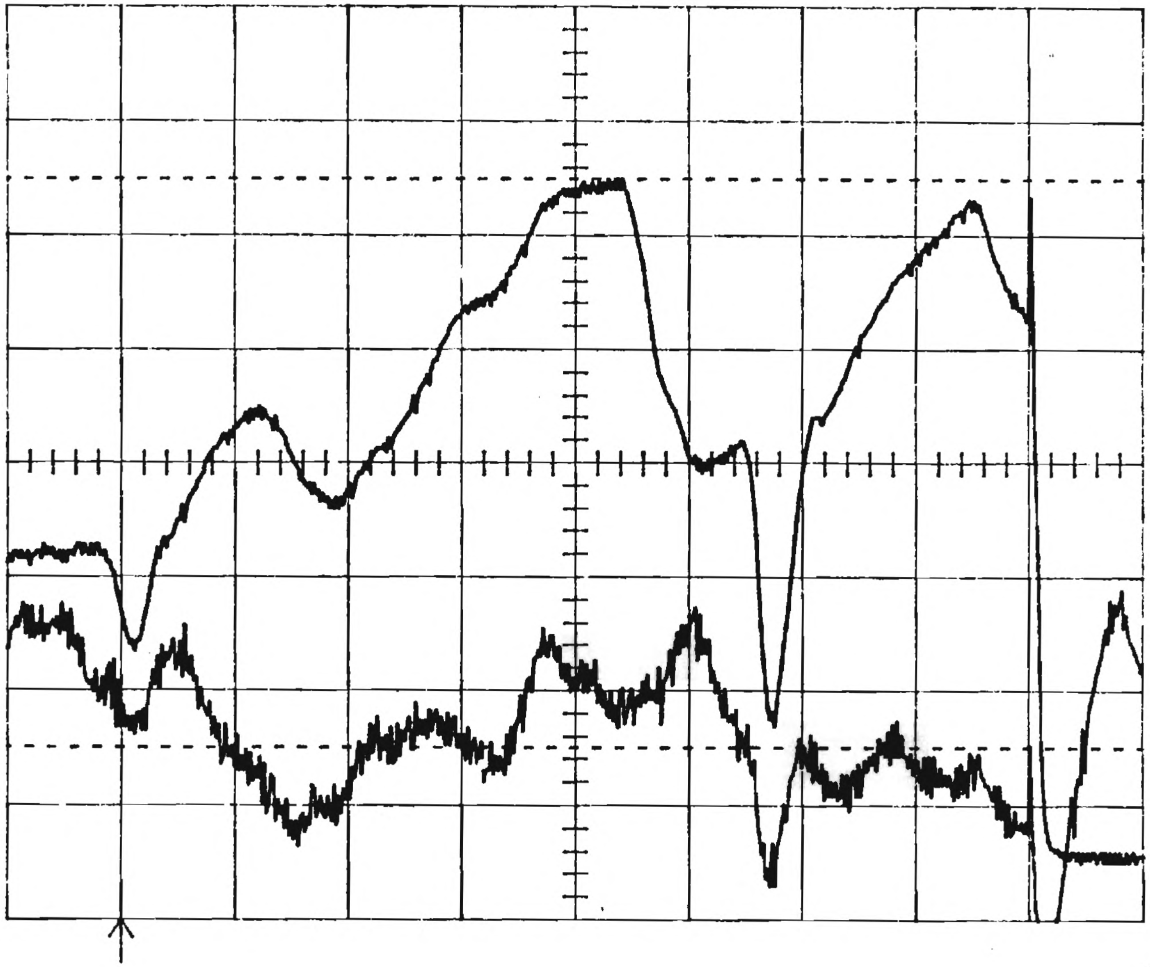

Channel 1 East
.1 ms 1 V K.S.

Channel 2 West
.1 ms .2 V I.S.

Ch 1 1 V ~
T/div .1 ms Ch 2 .2 V ~
Trig .49 V + EXT <

E: -36.7° 1000
r=4.00cm

W: +36.7° 1000

n-l Plasma Potential Structures

Main
Menu

1v

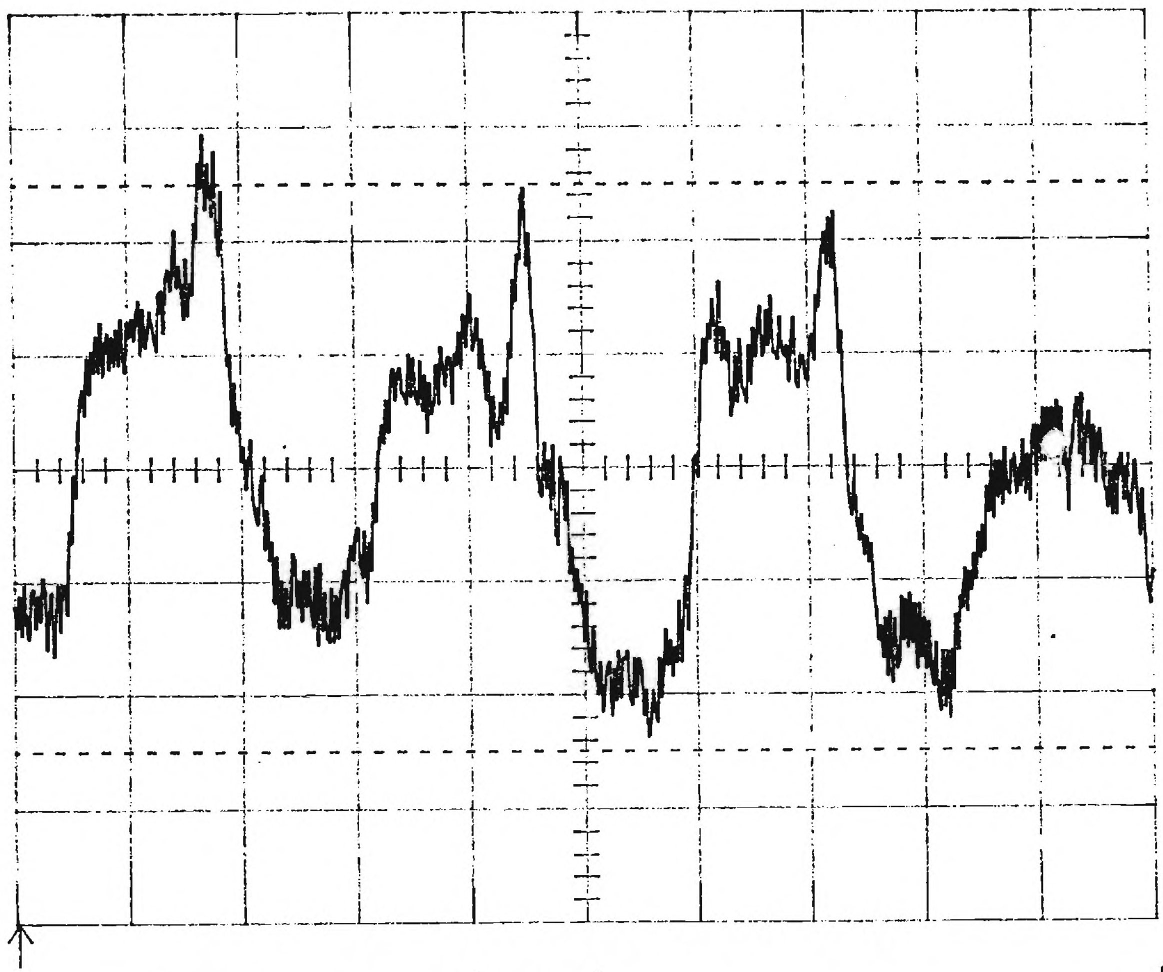

Channel 1 West KS
.2 ms .2 V 15 cm = 15…
18.1° = +2…

Hammer on continuously

0V can + mid

.60 mA can → gnd

Ch 1 .2 V ~
T/div .2 ms Ch 2 20 mV =
Trig 1.69 V + EXT <

[illegible] Ion density Structures

Now look at Ion Saturation

-94.8 V battery box bias

Main
Menu

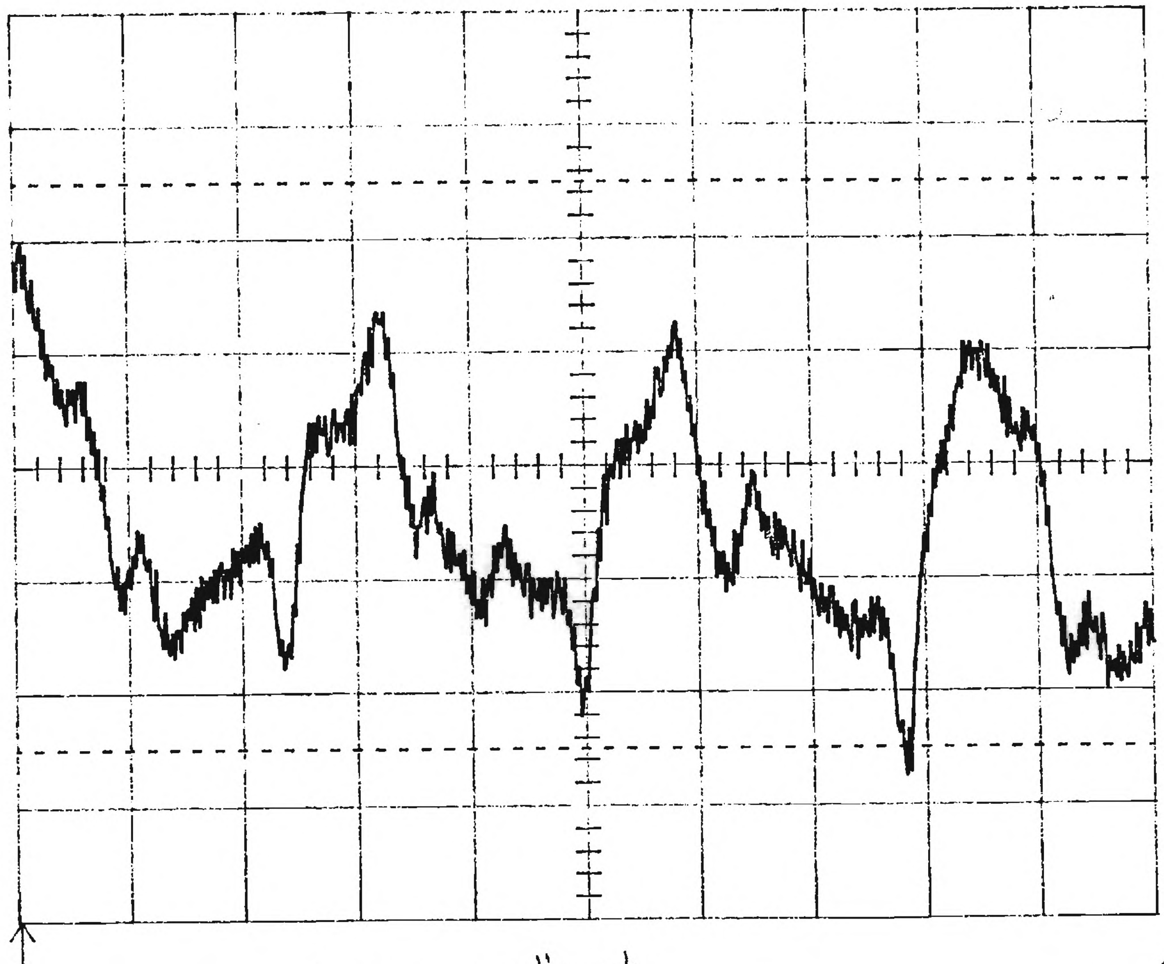

Channel 1 West
.2 ms .1 V I.S

15 cm = 150

18.1° = 1.2 c

Hammer continuously

0V can + mid

~.62 mA can -> gnd

Ch 1 .1 V ~
T/div .2 ms Ch 2 20 mV =
Trig 1.69 V + EXT <

Potential Structures

Ar →

He →

(10x the freq)

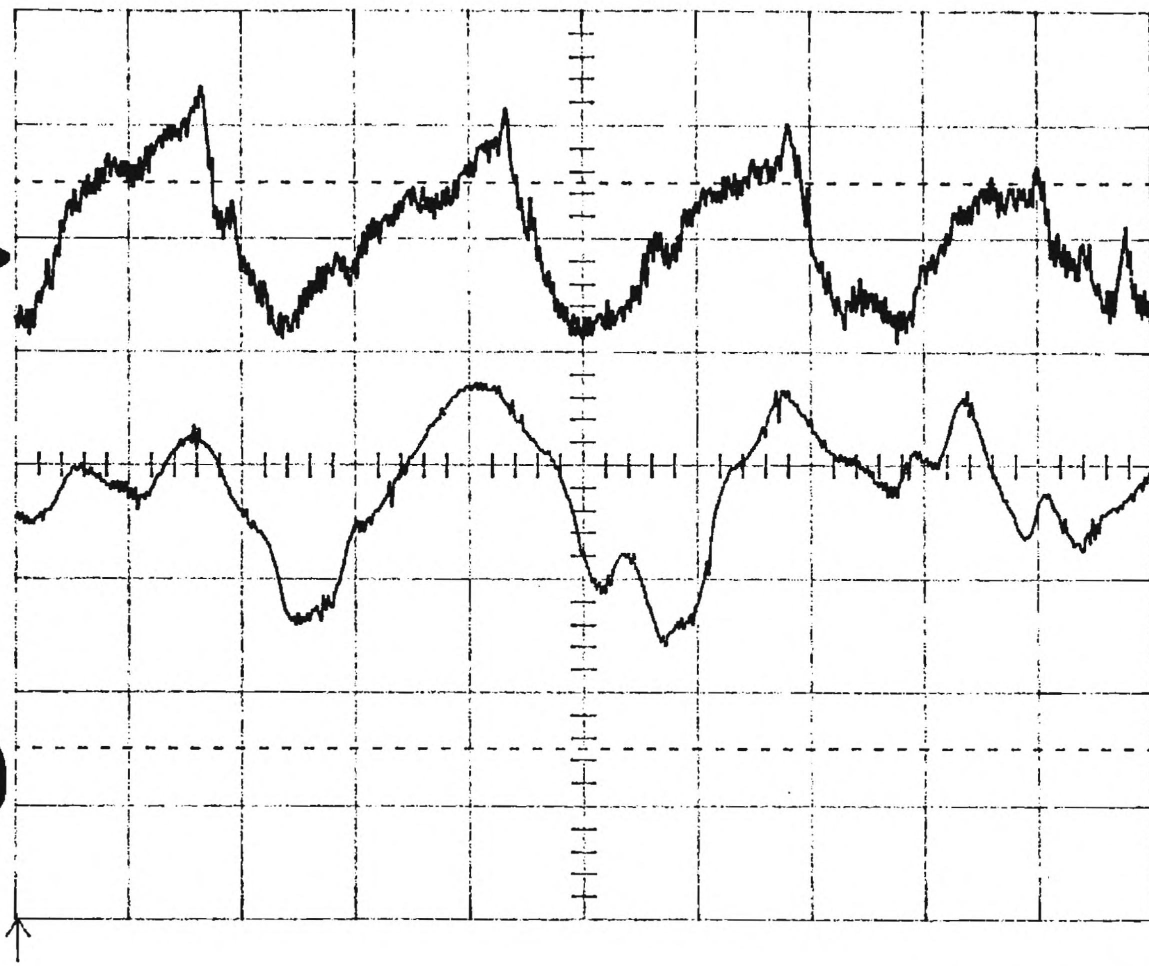

Argon

Memory D
.2 ms .5 V

West
K.S.
15 cm
18.1°

Helium

Channel 1
20 µs .5 V

West
K.S.
15 cm
18.1°

Ch 1 .5 V ~
T/div 20 µs Ch 2 20 mV =
Trig 1.69 V + EXT <

0 V can + mid

non-stochastic (survived 200 averages) waves

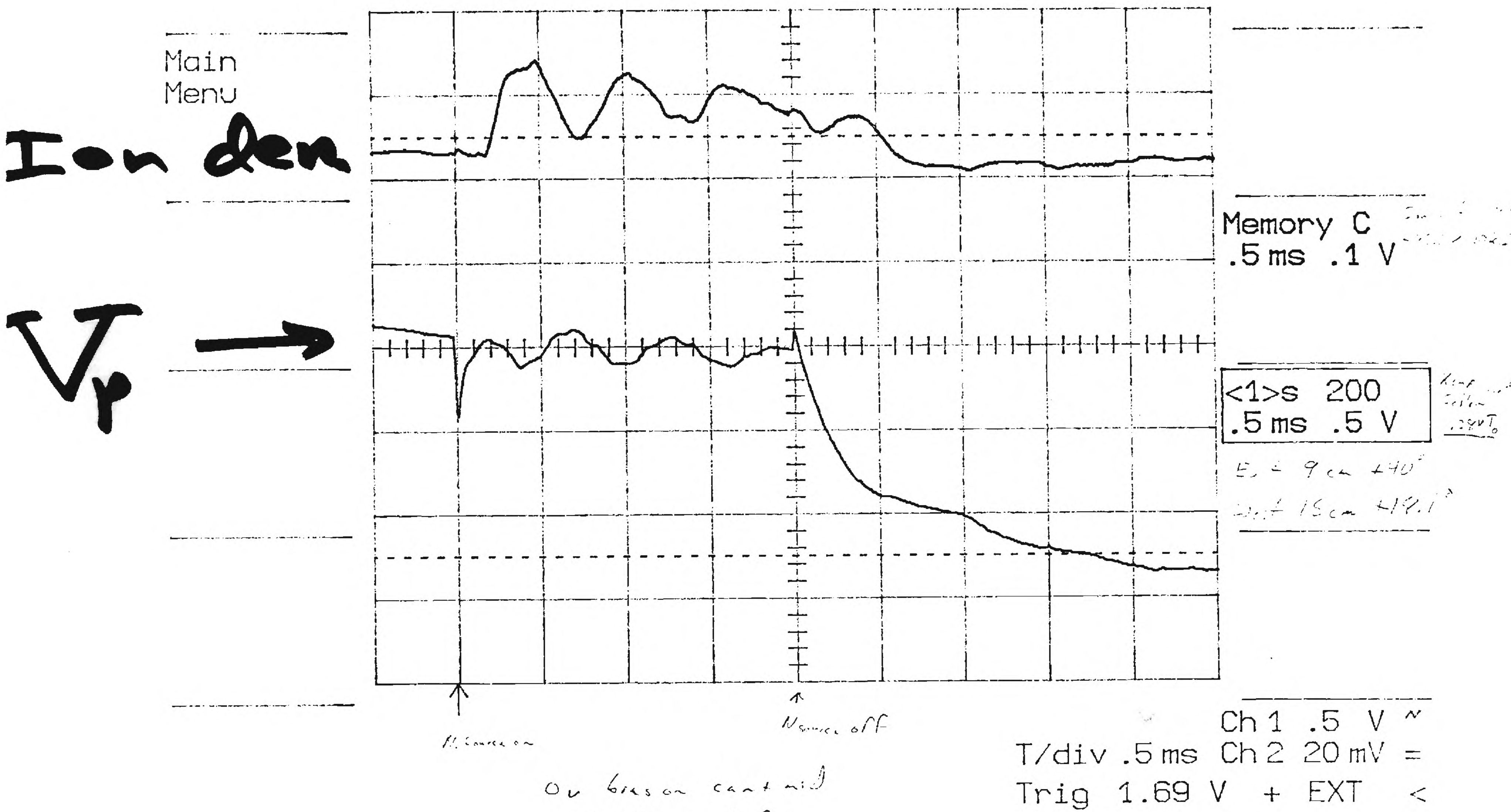

Ov bias on cant mid
.36 mA current from
centroid to gnd